



**5th International Conference on
Imaging Technologies in Biomedical Sciences**
*From Physiology and Cellular Biology
to Pathology through Imaging*

13-16 September 2009

**Milos Conference Center G.Eliopoulos
Milos Island, Greece**

TOPICS

- **Current Development in Imaging Technologies**
- **Hardware Components, Data Acquisition and Reconstruction**
- **Simulation Techniques**
- **Radiopharmaceuticals and Contrast Media**
- **Experimental and Small Animal Imaging**
- **Clinical Imaging (PET, SPECT, CT, MRI) and Multimodalities**
- **Image Visualisation and Processing**
- **Image Interpretation and Tele-Imaging**
- **New Ideas**

Conference Co-Chairmen

Michael GORIS (Stanford University, USA)

Andrew TODD-POKROPEK (University College London, UK)

Book of Abstracts

Organized by the :

Institute of Accelerating Systems and Applications (IASA)

and the

National & Kapodistrian University of Athens

<http://www.iasa.gr/itbs09>

Sponsored by:

S&B Industrial Minerals S.A. and the Greek Ministry of National Education and Religious Affairs

ITBS
2009

5th International Conference on
Imaging Technologies in Biomedical Sciences
From Physiology and Cellular Biology
to Pathology through Imaging

13-16 September 2009

Milos Conference Center G.Eliopoulos
Milos Island, Greece

TOPICS

- **Current Development in Imaging Technologies**
- **Hardware Components, Data Acquisition and Reconstruction**
- **Simulation Techniques**
- **Radiopharmaceuticals and Contrast Media**
- **Experimental and Small Animal Imaging**
- **Clinical Imaging (PET, SPECT, CT, MRI) and Multimodalities**
- **Image Visualisation and Processing**
- **Image Interpretation and Tele-Imaging**
- **New Ideas**

Conference Co-Chairmen

Michael GORIS (Stanford University, USA)

Andrew TODD-POKROPEK (University College London, UK)

International Scientific Committee

H. BONET (National Institute for Radioelements, Belgium)
I. BUVAT (Universite Pierre et Marie Curie, Paris, France)
A. CHATZIOANNOU (UCLA, USA)
Y. DECLAIS (IPNL, Lyon, France)
M. DEFRISE (Vrije University, Belgium)
N. GIOKARIS (University of Athens, Athens, Greece)
M. GORIS (Stanford University, USA)
C. HALLDIN (Karolinska Institute, Sweden)
M. HOFMANN (University of Hannover, Germany)
R. ITTI (University Claude Bernard, France)
W. KNAPP (Hannover Medical School, Germany)
B. KNOOP (Hannover Medical School, Germany)
P. LECOQ (CERN, Geneva, Switzerland)
P. Le DU (CEA, Saclay, France)
G. KONTAXAKIS (Univ. Politecnica de Madrid, Spain)
D. MAINTAS (Institute of Isotopic Studies, Athens, Greece)
J. MAUBLANT *(Centre Jean Perrin, Clermont-Ferrand, France)
S. MAJEWSKI (JLab, USA)
K. NIKITA (National Technical University of Athens, Greece)
R. PANI (University of Rome "La Sapienza", Italy)
G. PAGANELLI (European Institute of Oncology, Milano, Italy)
P. RIGO (Centre Hospitalier Princesse Grace, Monaco)
M. SCHNEEGANS (LAPP, Annecy-Le-Vieux, France)
E. STILIARIS (University of Athens, Athens, Greece)
J.-N. TALBOT (Hopital Tenon, Paris, France)
A. TODD-POKROPEK (University College of London, UK)
S. ZIEGLER (T.U. Muenchen, Germany)

Local Organising Committee

D. MAINTAS, Chair (Institute of Isotopic Studies, Athens, GR)
N. GIOKARIS, Scientific Secretary (University of Athens & IASA, GR)
S. ARCHIMANDRITIS (N.C.S.R. "Demokritos", GR)
N. KARATZAS (University of Thessaloniki, GR)
G. KASTIS (National Academy of Athens, GR)
K. NIKITA (National Technical University of Athens, GR)
E. STILIARIS (University of Athens, GR)
N. ZARIFE, Secretariat (IASA, Athens, GR)

Organized by the :

Institute of Accelerating Systems and Applications (IASA)

and the

National & Kapodistrian University of Athens

<http://www.iasa.gr/itbs09>

Information

Institute of Accelerating Systems and Applications (IASA)

P.O. Box 17214, Athens, 10024 Greece

Tel: +30 210 7257533, Fax: +30 210 7295069

itbs09@iasa.gr

Sponsored by:

S&B Industrial Minerals S.A. and the Greek Ministry of National Education and Religious Affairs

ITBS

2009

**Imaging Technologies in Biomedical Sciences
delegates at MILOS Hellenic island
SPECIAL ANNOUNCEMENT**



LECTURE BY ROLAND ITTI AND DANIELLE MESTAS AT 17.30 PM

A MEMORIAL CEREMONY

will be held

on Sunday September 13th at 01:30 pm

for JEAN MAUBLANT Chairman of the Dept.

of Nuclear Medicine of the University

of Clermont-Ferrand, France.

His premature death is deeply regretted..

ALL ARE WELCOME !

Thoughts have to be sent to E mail: netcompublishing@gmail.com press agency,

It will be published in the POSITRON issue at EANM 2009 Barcelona.

Donations can be made through

the conference website, <http://www.iasa.gr/itbs2009/index.html>.

ITBS09 PROGRAM

*George Eliopoulos Conference Centre
Milos Island, Greece
13-16 September, 2009*

	Sun 13-SEP	Mon 14-SEP	Tue 15-SEP	Wed 16-SEP
09:00 - 11:00		Session IIa	Session IIIa	Session IVa
		Coffee Break	Coffee Break	Coffee Break
11:30 - 13:30		Session IIb	Session IIIb	Session IVb
	Registration			
16:30 - 19:30	Session I OPENING Session & Introductory Talks	Session IIc	E X C U R S I O N	POSTER Session Session IVc CLOSING Talks
	Welcome Reception			BANQUET

Registration

Sunday, 13 September 2009 (afternoon)

15:00-16:30 *George Eliopoulos Conference Center, Milos Island*

Session I: OPENING Session

Sunday, 13 September 2009 (afternoon)

Time	Speaker	Title
16:30-17:00	D. Maintas (President of the Organizing Committee) Chr. Kittas (Rector of the University of Athens)	WELCOME
17:00-17:45	Roland Itti and Danielle Mestas	Lecture In Memory of Jean Maublant
	Co-Chairmen of the ITBS09 Scientific Committee Lectures	
17:45-18:30	M. Goris (Stanford)	Clinical Validating of Diagnostic Procedures
18:30-19:15	A. Todd-Pokropek (UCL)	Research and Development in Medical Imaging: Darwin's Theory about Product Development

Welcome Reception

Sunday, 13 September 2009 (afternoon)

19:30-21:00 George Eliopoulos Conference Center, Milos Island

Session IIa

Monday, 14 September 2009 (morning)

Time	Speaker	Title
09:00-09:45	Ch. Halldin (Karolinska)	PET in Drug Development (Invited Lecture)
09:45-10:00	R. Fulton	Imaging the awake rat brain with microPET, head tracking and motion correction
10:00-10:15	M. Tornai	Overview and preliminary results of a 3D Multi-Modality dedicated Molecular SPECT/CT breast imaging system
10:15-10:30	S. Beer	High-resolution PET in plants
10:30-10:45	F. Boisson	1D gamma counting approach to study radiopharmaceutical kinetics
10:45-11:00	M. Salouti	A new method to estimate Tumor/non-Tumor uptake based on Scintigraphic imaging to avoid killing the animal models

Session IIb

Monday, 14 September 2009 (morning)

Time	Speaker	Title
11:30-12:15	J.N. Talbot (Paris)	The New PET Radiopharmaceuticals (Invited Lecture)
12:15-12:30	S. Balogova	Fluoromethylcholine (18F) (FCH) PET/CT for the detection of hepatocellular carcinoma (HCC) in patients with a chronic liver disease and liver nodules and for staging hepatocellular carcinoma: prospective comparison with FDG (18F) PET/CT
12:30-12:45	C. Houzard	Hybrid Imaging in 2009: the nuclear medicine physician's point of view
12:45-13:00	M. Panagiotidis	Clinical experience with 18FDG-PET/CT in the public sector: Two thousand and one hundred patients findings in a large Greek tertiary hospital
13:00-13:15	A. Travade	Breast specific gamma imaging (bSgi) clinical use in France
13:15-13:30	S. Mardani Samani	Automatic identification of needle's entrance point and angle in Vertebroplasty

[Back](#)

Session IIc

Monday, 14 September 2009 (afternoon)

Time	Speaker	Title
16:30-16:45	L. Strauss (DKFZ)	Modeling in PET Studies (Invited Lecture)
16:45-17:00	C. Chauvet	Simultaneous analysis of myocardial perfusion SPECT and coronary CT angiography with a new integrated software: Feasibility study
17:00-17:15	B. Frish	ClearPEM-Sonic, a combined positron emission mammograph and ultrasound scanner
17:15-17:30	J. Dang	Development of anthropomorphic phantoms for combined PET-Ultrasound elastography breast imaging
17:30-17:45	M. Andreou	Evaluation of the positioning setup accuracy in prostate radiotherapy using an a-Si flat panel portal imaging device: The Aretaieion University Hospital experience
17:45-18:00	C. Maintas	Attenuation- or non-attenuation correction: Clinical Data
18:00-18:15	C. Giannopoulou	Utility of additional neck 18FDG-PET/CT images in patients with known or suspected neck malignancy
18:15-18:45	A. Todd-Pokropek (UCL)	Some Issues in Medical Imaging: State of the Art and Future Prospects

Session IIIa

Tuesday, 15 September 2009 (morning)

Time	Speaker	Title
09:00-09:45	N. Giokaris (UoA & IASA)	The Search for the Higgs Particle: Status and Prospects (Invited Lecture)
09:45-10:00	M. Bataglia	Low-flux imaging of biomedical samples with direct detection CMOS pixel sensors in low energy transmission electron microscopy
10:00-10:15	G. Llosa	Silicon photomultipliers, SiPM matrices and small animal PET
10:15-10:30	M. Dell Orso	A fast FPGA-based clustering algorithm for real time image processing

Session IIIb

Tuesday, 15 September 2009 (morning)

Time	Speaker	Title
11:30-12:15	B. Knoop (Hannover)	Multi-Centre Trials with PET: Physical Prerequisites (Invited Lecture)
12:15-12:30	K. Kacperski	Scatter correction in 201TI cardiac SPECT based on multiple energy windows data
12:30-12:45	K. Baum	Calibration and evaluation of a dual layer high dynamic range display for pathology detection tasks
12:45-13:00	S. Kolokytha	"Intelligent" CT: Optimizing image quality and reducing dose
13:00-13:15	S. Michopoulou	Intensity inhomogeneity correction in MRI of lumbar spine at 3T

[Back](#)

Session IVa

Wednesday, 16 September 2009 (morning)

Time	Speaker	Title
09:00-09:45	A. Olivo (UCL)	Advances in Phase Contrast Imaging (Invited Lecture)
09:45-10:00	B. Chen	Measuring trabecular bone orientation by diffusion tensor imaging
10:00-10:15	D. Thanasas	Reconstruction optimization for Gamma-Camera planar images from resistive chain readouts
10:15-10:30	A. Bonissent	Accelerated image reconstruction on a cluster of two AMD GPUs in CBCT with non-uniform detector geometry
10:30-10:45	F. Babapour	Fuzzy linear regression approach for estimation of photon escape probability from HPGe detectors

Session IVb

Wednesday, 16 September 2009 (morning)

Time	Speaker	Title
11:30-12:15	P. Guiderdoni and R. Itti (Lyon)	Art is me, Science is us : Are nucmed physicians the heirs of Claude Bernard's milieu interieur? (Invited Lecture)
12:15-12:30	M. Pop	Characterization of cardiac electrophysiology in pathologic hearts using optical imaging, MRI and computer modelling
12:30-12:45	G. Kovacs	Sinogram correction methods in MiniPET-II
12:45-13:00	Z. El Bitar	Accelerated three dimensional Monte Carlo image reconstruction technique in small animal SPECT
13:00-13:15	G. Christopoulos	Attenuation- or non-attenuation correction: Phantom Data

POSTER Session

Wednesday, 16 September 2009 (afternoon)

Time	Speaker	Title
16:30-18:00		POSTER Session

Session IVc: Closing Talks

Wednesday, 16 September 2009 (afternoon)

Time	Speaker	Title
18:00-18:45	R. Itti (Lyon)	Conference Summary
18:45-19:30	A. Todd-Pokropek (UCL)	Closing Talk

[Back](#)

Version 1.03 (updated on 07-SEP-2009, 20:00 EEST)

PART I

Oral Presentations

Session IIa

Imaging the awake rat brain with microPET, head tracking and motion correction

R. Fulton, S. Meikle, A. Kyme, V. Zhou, M. Akhtar, M. Kassiou, K. Popovic, I. Karlsson.

Brain and Mind Research Institute, University of Sydney, Australia.

Small laboratory animals are normally anesthetized during microPET imaging to avoid motion artifacts. However anesthesia induces changes in blood flow and other functional parameters that alter radiotracer uptake and prevent investigation of the brain in its normal state. There is therefore interest in techniques for imaging the awake rat brain with PET. The approach that we have investigated is to allow the animal complete freedom to move its head within the field of view of a conventional small animal PET scanner, and to apply motion tracking and motion correction techniques to obtain images free of motion effects.

Materials and Methods:

Telemetric core body temperature probes (TA-F20, Data Sciences International) were surgically implanted into two 4 week old female Sprague-Dawley rats for continuous monitoring of core body temperature during training and imaging procedures. After a 5 day recovery period, 20-min training sessions were conducted twice daily for 4 days to acclimatize the animals to an open-ended tubular burrow mounted in the microPET scanner (Focus 220, Preclinical Solutions, Siemens Medical Solutions USA, Inc.).

Prior to microPET imaging rats were injected in the tail vein with 60 MBq of [18-F]FDG, and allowed to rest for a 20-min uptake period, prior to being placed into the burrow with the head protruding into the scanner field of view. No restraint was applied other than a plug to prevent backward motion along the burrow. This arrangement appeared to be well tolerated by the rats, with their core body temperature never exceeding 39°C, which would indicate an unacceptable degree of stress. Each rat underwent 3 separate imaging sessions over a 4 week period. Imaging sessions comprised a 10 min emission scan, followed immediately by a 20 min transmission scan. One rat terminated some sessions prematurely by exiting the burrow.

Head pose in microPET coordinates was recorded 30 times per second throughout the imaging sessions with an optical motion tracking system (Micron Tracker, Claron Technology Inc.). Motion correction was applied to both emission and transmission listmode scans by applying transformations derived from the synchronized pose data to event lines of response. Motion corrected sinograms were corrected for attenuation, rebinned to 2D using FORE, and reconstructed with OSEM.

Results:

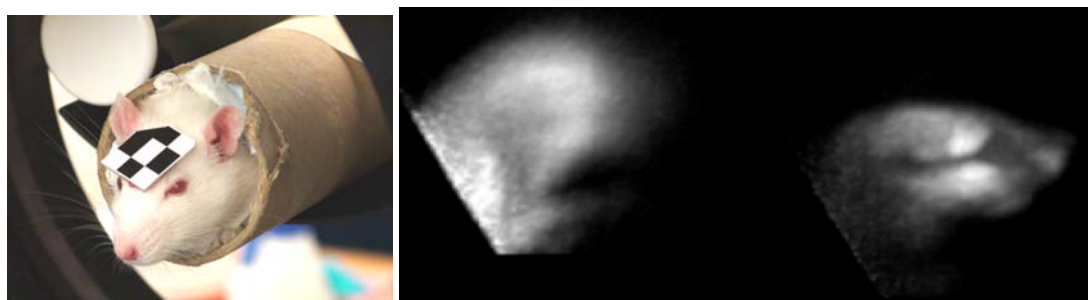


Fig 1. **Left:** Rat in burrow during a microPET scan. The motion tracking target is seen affixed to the fur. **Right:** Maximum intensity projection (MIP) images of rat's head without motion correction (left) and with motion correction (right). Motion correction dramatically improved image clarity.

Conclusions:

These experiments show that high quality microPET brain images can be obtained in conscious rats without apparent stress to the animal using motion tracking and a motion correction algorithm. We hope this new capability will facilitate behavioural, activation and other experiments that require the animal to be awake. We are adapting aspects of our technique to clinical PET applications for use in patients (e.g. young children) likely to exhibit uncontrolled head motion during the scan.

OVERVIEW AND PRELIMINARY RESULTS OF A 3D MULTI-MODALITY DEDICATED MOLECULAR SPECT/CT BREAST IMAGING SYSTEM

MP TORNAI^{1,2,3}, RL MCKINLEY⁴, P MADHAV^{1,2}, SJ CUTLER^{1,2}, DJ CROTTY^{1,2}, KL PEREZ^{1,3}

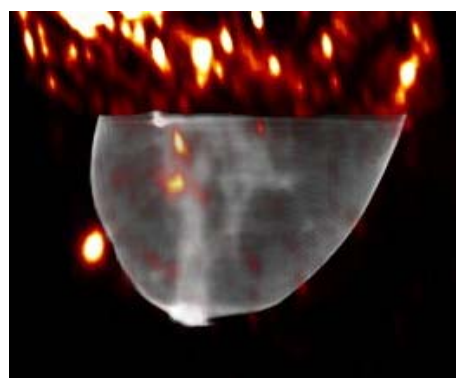
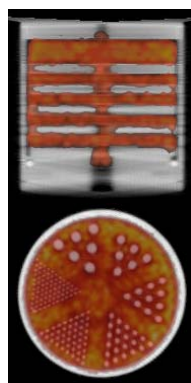
¹ Department of Radiology, Duke University Medical Center, Durham, NC 27710, USA

² Department of Biomedical Engineering, Duke University, Durham, NC 27708, USA

³ Medical Physics Graduate Program, Duke University, Durham, NC 27710, USA

⁴ Zumatek, Inc., Research Triangle Park, Durham, NC 27709, USA

Purpose: We are developing a high performance SPECT/CT hybrid imaging system targeted specifically towards imaging normalcy, disease, and disease (re)staging in the human breast. Some goals include: improving patient comfort and reducing absorbed radiation dose during imaging; detecting and characterizing earlier stage breast cancers; monitoring therapeutic responses. This common field-of-view system provides semi-quantitative 3D functional and anatomical coregistered images of a pendant, uncompressed breast. **Methods:** The SPECT subsystem uses a compact CZT camera with 6% FWHM at 140keV to enable fully-3D acquisition trajectories that closely contour any breast, minimize spatial resolution degradation, overcome distortions due to inadequate sampling, and allow detection of lesions on the chest wall. The CT subsystem uses a quasi-monochromatic 15% FWHM at 36keV fully-3D cone-beam x-ray source impinging on a CsI(Tl) detector, and is restricted to circular rotation. Effects of signal cross-talk between the systems are characterized. Energy resolution and spectral characteristics are demonstrated, along with imaging of mini-geometric resolution and sampling phantoms. Human observer studies contrast standard 2D scintimammography and digital x-ray mammography with this SPECT/CT system. Patient studies include women with surgically confirmed breast cancer. **Results:** The band-limited x-ray spectrum allows dramatically reduced radiation dose imaging. Minimal cross-contamination was observed between subsystems. Imaging responses of geometric phantoms display fine resolution, excellent 3D sampling capabilities, and semi-quantifiable results for emission/transmission imaging. Observer results with SPECT/CT statistically significantly outperform 2D imaging modalities in small object visualization studies. Patient imaging studies clearly illustrate small lesion visualization, and excellent coregistration between SPECT/CT subsystems, though physical CT subsystem constraints limit visualization of the posterior breast. **Conclusion:** With the elimination of overlapping tissues through fully-3D imaging, complementary SPECT/CT images improve lesion localization versus conventional 2D imaging modalities. This class of dedicated SPECT/CT system promises greatly improved visualization of the full breast. The complementary information from anatomical and structural imaging can both guide lesion localization for subsequent analysis, and monitor therapeutic progress over the long term.



Figures: (LEFT) Photograph of the hybrid patient bed suspending an anthropomorphic breast phantom. Orange directional arrows indicate directions of motion for each component. (MIDDLE) OSEM reconstructed, registered and fused slices taken through mini-disk (5mm disks and spaces) and mini-cold rod (rods range from 1.1 to 4.7mm) phantoms, with CT component in grey and SPECT in "hot" color scales. (RIGHT) Reconstructed sagittal slice from a human subject hybrid SPECT/CT scan using ^{99m}Tc-mibi including: external SPECT/CT fiducial marker; breast-internal SPECT signals show surgically confirmed DCIS; biopsy clip at posterior breast in reconstructed CT volume; cardiac uptake of SPECT tracer.

Disclosure: MPT is an inventor of this technology, and is named as an inventor on the patent for this technology applied for by Duke. If this technology becomes commercially successful, he and Duke could benefit financially.

High-resolution PET in plants

S. Beer¹, J. Bühler², T. Hombach², S. Jahnke², H. Larue¹, C. Parl¹, G. Roeb², U. Schurr², M. Streun¹ and K. Ziemons¹

¹Central Institute for Electronics, ²ICG-3: Phytosphere, Forschungszentrum Jülich, 52425 Jülich, Germany

Positron emitters like ¹¹C, ¹³N or ¹⁸F are widely used in clinical diagnosis and animal studies, but can also be applied to noninvasively study metabolic and physiological functions in plants. ¹¹CO₂, for example, can be applied to leaves to trace the movement of photosynthetic products in plants. The monitoring of the labeled compounds within the intact plant has been realized so far by a set of collimated detectors, by detectors in coincidence mode [1] or by a planar camera [2]. These studies are limited to plants or plant parts growing in a planar fashion.

A dedicated high-resolution PET system, the Plant Tomographic Imaging System (PlanTIS)[3], with a spatial resolution of ~1.3 mm is used now in our institutes to study the dynamics of carbon supply from source leaves to different plant organs including roots in soil or bulky organs such as beets or fruits. The scanner is based on ClearPET technology [4] and consists of LSO and LuYAP scintillator crystals in phoswich configuration which are coupled directly to position sensitive PMT's. Data are acquired in list mode and are reconstructed iteratively.

We will introduce some of the basic concepts behind the use of short-lived radiotracers in plant physiology with respect to high-resolution PET and give a few application examples. Since the use of high-resolution PET for this kind of application is quite new, we will discuss the main challenges of this new application in comparison with small-animal PET, e.g. the requirements of deadtime correction or the influence of radioactivity from outside the field of view due to the gas supply.

The initial performance of the scanner and first applications, like a 5 minute scan of barley roots in soil after ¹¹C uptake by the leaves (Fig.1) will also be presented.

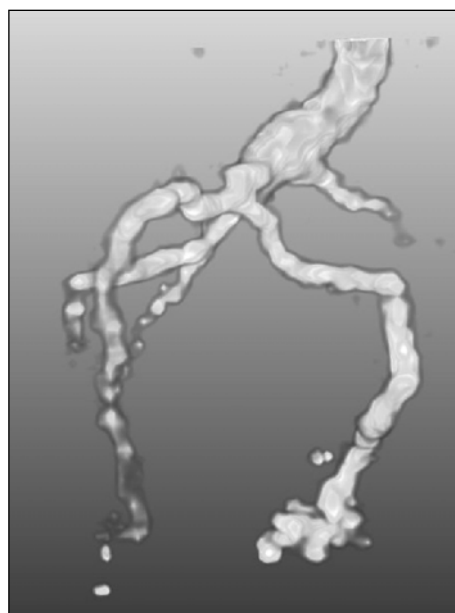


Fig. 1 PET scan of a barley root in soil after ¹¹CO₂ application to the leaves

References

- [1] Minchin P E H, Thorpe M R 2003 Using the short-lived isotope ¹¹C in mechanistic studies of photosynthate transport *Funct. Plant Biol.* **30** 831-41
- [2] Kawachi N, et al. 2006 Kinetic analysis of carbon-11-labeled carbon dioxide for studying photosynthesis in a leaf using Positron Emitting Tracer Imaging System *IEEE Trans. Nucl. Sci.* **53** 2991-7
- [3] Jahnke S, et al 2009 Combined MRI-PET dissects dynamic changes in plant structures and functions *Plant J*, doi: 10.1111/j.1365-313X.2009.03888.x
- [4] Ziemons K, et al 2005 The ClearPETTM project: development of a 2nd generation high-performance small animal PET scanner *Nucl. Instr. Meth. A* **537** 307-11

1D Gamma Counting Approach to Study Radiopharmaceutical Kinetics

F. Boisson¹, V. Bekaert¹, Z. El Bitar¹, J. Steibel² and D. Brasse¹

¹ Institut Pluridisciplinaire Hubert Curien. UMR 7178 - CNRS/IN2P3 and UDS. BP 28 - 23, rue du Loess. 67037 STRASBOURG Cedex 02, France.

² Laboratoire d'Imagerie et de Neurosciences Cognitives, UMR 7191 - CNRS/IN2P3 and ULP - 12, rue Goethe, 67000 STRASBOURG, France

I. INTRODUCTION

Current researches based on small animal model are dedicated to functional cerebral imaging which represents a fundamental tool to understand the mechanisms involved in neurodegenerative diseases. In the radiopharmaceutical development approach, the main challenge is to measure the radioactivity distribution in the brain of a subject with good temporal and spatial resolutions in order to investigate the behaviour of new radiopharmaceuticals inside the injected subject. In the case where the isotope is a single photon emitter, the measurements can be achieved using a Single Photon Emission Computed Tomography (SPECT) system. However, with such imaging systems, compromises have to be made regarding the spatial resolution and the detection efficiency. Two different ways have been investigated to improve both spatial resolution and detection efficiency: a multipinhole approach and the slit-slat collimation approach using in general CdZnTe as the detection material.

In this manuscript, we present a 1 D gamma counter to obtain both high detection efficiency and good spatial resolution mainly dedicated to the study of radiopharmaceutical kinetic with a low cost and a small footprint. However, the price to pay is the loss of one dimension spatial information.

II. MATERIALS AND METHODS

The detector consists in a cerium doped yttrium aluminum perovskite crystal (YAP:Ce) of $18.4 \times 18.4 \times 10 \text{ mm}^3$ coupled to a MultiAnode PhotoMultiplier Tube (MAPMT) associated to a dedicated electronic. The MAPMT from Hamamatsu Corp. has an active area of $18.4 \times 18.4 \text{ mm}^2$ and is composed of 64 channels of $2 \times 2 \text{ mm}^2$ with a pitch of 2.3 mm. The crystal is coupled to the MAPMT using optical grease ($n = 1.465$).

The YAP crystal is segmented into strips of 570 μm wide optically separated by a layer of 5 microns reflector. The segmented YAP crystal presents an alternative to obtain an intrinsic spatial resolution less than one millimetre. The price to pay is the loss of one dimension spatial information.

In order to match the YAP segmentation, the collimation is performed using 33 tungsten slats to keep the one-dimensional spatial information given by the 32 YAP strips. Each tungsten slat is 100 μm thick representing a good compromise between the effect of the septal penetration and the introduced detection dead space.

However, the collimation height had to be determined to optimize the detection efficiency in each transverse slice and reduce the septal penetration effect on the spatial distribution. Several Monte Carlo simulations using GEANT4 were performed to investigate the optimized collimation height.

III. RESULTS AND DISCUSSION

For one event, the 64 MAPMT readout signals are recorded and a clusterization algorithm is used to extract the position and the energy of the event. In average, the cluster consists in 18 ± 5 channels of the MAPMT. The resulting energy spectrum leads to an energy resolution of 29.7 % calculated using a Gaussian fit where the X-ray fluorescence of tungsten and lead are taken into account.

The 28 central strips are clearly visible. However, the first 2 strips and the last ones are not distinguished due to edge effects. To keep the entire FOV of the detector, the edge strips are combined to form two broad areas. The uniformity correction leads to a flat distribution with a standard deviation of 1 %.

According to the position of the brain regarding the experimental setup, the optimal collimation height is found to be equal to 40 mm.

The projection of the 1.5 mm diameter ⁵⁷Co source located at 20 mm from the CEF provides a FWHM equal to 1.75 mm, which leads to a spatial resolution of 0.9 mm after the correction of the source beam size.

The collimation detection efficiency varies as the inverse of the distance between the point of emission and the detector.

Knowing the activity of the source or its velocity, one of these two parameters can be estimated from the measurement using the count rate.

IV. CONCLUSION

The use of a multi-slit gamma counter consisting in a highly segmented YAP:Ce crystal combined to a dedicated collimation leads to a spatial resolution below one millimetre with a detection efficiency of 0.064 % for a 1.5 mm diameter source located at a distance of 1 cm. A 2D projection can be obtained using a spin rotation of the entire system.

The current proposed approach is an alternative to the multipinhole SPECT system for screening purposes. Combined with a microCT system, the 1D gamma counter gives a low cost tool to investigate new radiopharmaceutical mainly dedicated to brain studies.

This paper gives preliminary results on the intrinsic performances of the device. More investigations have to be performed to evaluate the system in preclinical studies.

A New Method to Estimate Tumor/non-Tumor Uptake Based on Scintigraphic Imaging to Avoid Killing the Animal Models

M. Salouti^a, H. Rajabi^b, M. H. Babaei^c, M.J. Rasaei^d, F. Saghatchi^e

^aDept. of Biology, School of Sciences, Islamic Azad University, Zanjan Branch, ^bDept. of Medical Physics, School of Medical Sciences, Tarbiat Modarres University, ^cDept. of Radioisotope, Nuclear Research Center, Atomic Energy Organization of Iran, ^dDept. of Medical Biotechnology, School of Medical Sciences, Tarbiat Modarres University, ^eDept. of Radiology, School of Medical Sciences, Zanjan University of Medical Sciences
E-mail address of main author: saloutim@yahoo.com

Introduction

Tumor imaging using monoclonal antibodies carrying radioisotopes is a promising approach toward improving early diagnosis of cancer in nuclear medicine. A biodistribution study in animal models bearing tumors is one of the most important procedures in evaluation of fractional uptake of radiopharmaceuticals in the tumor and non-tumor organs. This examination is often performed on rodents to extrapolate potential doses of these agents to humans. It is obvious that if we can design a non-invasive method to evaluate biodistribution, the need for large amount of monoclonal antibody (which is expensive and very difficult to produce) and the number of animals to be sacrificed (due to moral considerations) is decreased. The aim of this study was to develop a new method to determine activities that accumulated in the main organs as well as tumor without killing the animals based on scintigraphy images taken by a double head gamma camera.

Material and Methods

The MAb PR81 that recently was produced against human breast tumor, radiolabeled with ^{99m}Tc. The complex was injected (20 µg PR81, 400µCi activity for each mouse) to 20 BALB/c mice with xenograft breast tumor (weight 25-35 g). The anterior and posterior images of mice were taken 16 hours after ^{99m}Tc-PR81 injection using a double head gamma camera. The images were transformed to PC after converting them to interfile format. Then the anterior and posterior images of each mouse were conjugated using the designed software. After that with drawing ROI around each organ as well as tumor, the counts were obtained considering calibration and background contribution. Then the mean and SD of counts was calculated for each organ. Meanwhile, the mice were killed, the organs dissected and were counted individually using a well counter and the mean and SD of counts was calculated for each organ. Finally, the measurements obtained by the both ways for tumor and main organs were compared. The figure 1 shows a view of designed soft ware.

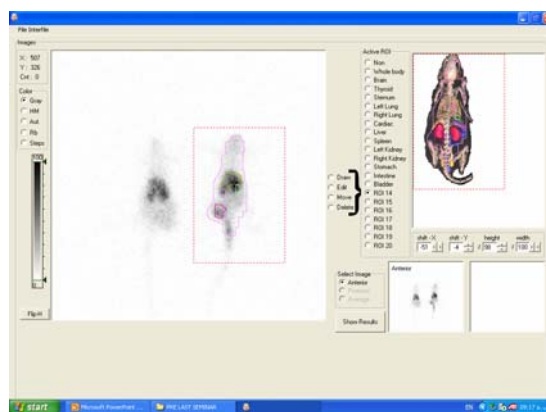


Figure1: A view of software designed to estimate tumor and main organs uptake

Results

The comparison of the results obtained by both procedures showed that there is a significant difference between the measurements. It means that the new method cannot be replaced with the invasive one to estimate the absolute activity of each organ. This is mainly due to overlapping of the organs that causes error in calculations of accurate activity of each organ. But the new method can be used to compare the relative activity of tumor and main organs in relation to each other in order to evaluate the quality of new radiopharmaceutical for targeting tumor as a basic parameter. The table 1 shows the results of count measurements obtained by the non-invasive and the invasive methods.

Table1: The count measuring result 16 hours after ^{99m}Tc -PR81 injection in tumor and main organs obtained by the invasive and software method

Organ	Invasive Method		Software Method	
	Mean(CPM)	SD	Mean(CPM)	SD
Liver	1322	105	1851	166
Kidney	1183	94	1657	149
Lungs	205	16	287	25
Heart	75	6	105	9
Spleen	362	28	506	45
Intestines	1729	138	2421	217
Thyroid	463	37	518	58
Tumor	958	76	1341	120

Conclusion

The new method can be used to compare fractional activities of tumor and main organs to evaluate the quality of any new smart radiopharmaceutical for targeting the tumor without killing the animals.

References

- [1] SALOUTI, M., RAJABI, H., BABAEI, M. H., RASAEI, M. J., A New Monoclonal Antibody Radiopharmaceutical for Radioimmunosintigraphy of Breast Cancer: Direct Labeling of Antibody and Its Quality Control, DARU (2006) 14(1): 14-19
- [2] STABIN, M.G., PETERSON, T.E., HOLBURN, G.E., Voxel-Based Mouse and Rat Models for Internal Dose Calculations, The Journal of Nuclear Medicine (2006) 47(4): 655-659

Session IIb

Fluoromethylcholine (18F) (FCH) PET/CT for the detection of hepatocellular carcinoma (HCC) in patients with a chronic liver disease and liver nodules and for staging hepatocellular carcinoma: prospective comparison with FDG (18F) PET/CT.

BALOGOVA S+, HUCHET V+, GUTMAN F+, KERROU K+, NATAF V+, MONTRAVERS F+, FARTOUX L++, BUMSEL F++, ANCEL D+++, GRANGE JD+++, ROSMORDUC O++, TALBOT JN+

+Department of Nuclear Medicine, Hôpital Tenon, AP-HP, et Université Pierre et Marie Curie, Paris, France.

++Departement of Hepatogastroenterology, Hôpital Saint Antoine, AP-HP, et Université Pierre et Marie Curie, Paris, France.

+++Departement of Hepatogastroenterology, et Université Pierre et Marie Curie, Paris, France.

AIM: We have shown in a proof-of-concept study that FCH was taken-up by HCC more frequently than FDG. The aim of this prospective study was to compare the diagnostic performance of FCH and FDG to detect HCC in 58 patients with chronic liver disease and nodule(s) and to compare the diagnostic performance of FCH and FDG PET/CT for staging HCC, according to its differentiation.

METHODS: 58 Patients which whom 34 with newly diagnosed (n=27) or recurrent (n=7) HCC were prospectively enrolled. HCC was assessed by histology in 29 cases (17 well-differentiated HCC) and by European Association for the study of the liver criteria in 5 cases. All patients underwent whole-body FCH PET/CT 10 min after injection of 4 MBq/kg and whole-body FDG PET/CT 1 h after injection of 5 MBq/kg FDG. On basis of histology and/or subsequent follow-up >6months 114 hepatic lesions and 10 extra-hepatic lesions were evaluable.

RESULTS: The 58 patients had 34 HCC, 4 cholangiocarcinoma, 2 liver metastasis of colon cancer, 14 liver adenoma and/or focal nodular hyperplasia, and 3 another benign hepatic lesion. Per patient performance of FCH & FDG for detecting presence of HCC, any positive result in another cancer being considered FP.

HCC per patient	Sensitivity	Specificity	PPV	NPV	Accuracy
FCH	27/34= 79%	13/24= 54%	27/38=71%	13/20=65%	40/58= 69%
FDG	23/34= 68%	17/24= 71%	23/30=77%	17/28=61%	40/58= 69%
McNemar's test	p=0.4	p=0.2			p>0.8

Evaluable sites were 124, of which 114 in the liver: 83 malignant and 31 benign. Of the 83 malignant sites, 13 were from non-HCC origin and 70 were HCC. 32 HCC lesions were well-differentiated.

HCC/HCAC overall sites	Sensitivity overall	Sensitivity well diff	Specificity	PPV	NPV	Accuracy
FCH	59/70=84%	30/32=94%	23/52=44%	59/88=67%	23/34=68%	82/122=67%
FDG	47/70=67%	19/32=59%	33/52=64%	47/66=71%	33/56=59%	80/122=68%
Mc Nemar's test	FCH=16 FDG=4 p=0.01	p<0.001	FCH=3 FDG=13 p=0.02			FCH=19 FDG=17 p>0.8

Overall, FCH was non-significantly more sensitive but less specific than FDG. In fact, of the 17 patients with well-differentiated HCC, 9 had a positive result with both FCH and FDG but 8 had a positive result with FCH only, while FDG was never positive alone (p<0.001). In contrast, FDG was more effective to diagnose cholangiocarcinoma or metastases. Furthermore, all photopenic FCH foci corresponded to malignancy. However FCH FP results were frequent in benign conditions: 7/8 patients with nodular focal hyperplasia (NFH). 1/6 patients with pure adenoma, and 1 patient with cholangitis who was the only FDG FP result in benign lesions.

CONCLUSION: FCH has an added value over FDG to stage HCC, in particular for liver sites in well-differentiated HCC. The indications that can be derived from the present study for FCH PET/CT in known HCC are:

- a first line examination for staging well-differentiated HCC
- a second line examination after FDG PET/CT in case of intermediate or poorly differentiated HCC, in particular when liver transplantation is scheduled or when FDG PET/CT is negative, but interpretation must be aware of FP results in NFH.

Hybrid Imaging in 2009: the nuclear medicine physician's point of view

C Houzard^{1,2}, D Maintas³, P.J. Valette¹, F Giammarile^{1,2}

¹ PAM d'imagerie Centre Hospitalier Lyon Sud France

² EA 37 38 - Faculté de Médecine Lyon sud UCB Lyon I

³ Institute of Radioisotopic Studies Athens Medical Center, Distomou 5-7 Maroussi Greece

Introduction The association of a CT scan (X-ray computerized tomography) with nuclear medicine scans, either PET (positron emission tomography), or conventional gamma-camera SPECT (single photon emission computerized tomography), allows integrating morphological and functional information on a single exam. This technological evolution is certainly very interesting, but should be carefully employed. Namely, artifacts in attenuation correction (and thus in SUV quantification) arising from CT algorithm, should be known and managed. Furthermore, it could be interesting to fully exploit the technical characteristics of CT scan, namely the possibility to inject intravenously iodinated contrast media in order to enhance image contrast. In this paper, we will report about technical aspects, clinical considerations and radioprotection issues of employing, in current clinical practice, contrast enhanced CT-scan during PET-CT study.

A preliminary phantom study showed that attenuation corrected PET images (CTAC) with our camera (Gemini Philips) were not affected by high atomic number, such as iodine, neither elevated density. A subsequent investigation, performed in our hospital during 18FDG PET-CT exams, evaluated the feasibility of contrast enhanced CT-scan for diagnosis purpose in 25 lymphoma staging. This in vivo prospective study showed no statistical difference for visual analysis and for SUVmax (maximum standard uptake value) on CTAC images, corrected by standard CT or iodine enhanced CT.

Materials and methods This retrospective study included 50 consecutives lymphoma patients (25 males and 25 females; mean age 46 ± 18 years) that performed 18F-FDG PET (5.2 MBq/kg) with our Gemini Philips camera. Images were acquired immediately after iodinated contrast enhanced CT-scan (100 ml of Iobitridol 350). Abnormalities, comparison with previous examinations and diagnostic conclusions were separately analyzed by a nuclear physicist and a radiologist on CTAC PET, CT and fusion images.

Results Enhanced CT scan showed less indeterminate data (N = 8/76) thus improving diagnosis accuracy. These results are confirmed by the literature data. A benefit is also obtained on logistic ("one stop shot") and radioprotection purposes.

Discussion In our institution, we realize since 2007 iodine contrast enhanced CT-scan during 18FDG PET-CT. Important quality factor results in an effective collaboration between radiologists and nuclear physicians, who learned slice imaging, with simultaneous interpretation of the images. Actually, in nuclear medicine centers equipped with multi-row CT combined with PET, CT with multiphase injection is used for diagnostic purpose (CTAC images are then obtained with a preliminary low dose non injected CT).

Similarly, the question of contrast enhanced CT is equivalent with SPECT-CT cameras in some indications.

Conclusion Recent technological evolution leads us to change nuclear medicine practices (i.e. iodine injection and slice imaging) for an optimized utilization of each side of hybrid imagery.

CLINICAL EXPERIENCE WITH 18FDG-PET/CT IN THE PUBLIC SECTOR: TWO THOUSAND AND ONE HUNDRED PATIENTS' FINDINGS IN A LARGE GREEK TERTIARY HOSPITAL.

Panagiotidis M, Giannopoulou C, Rondoyianni P, Exarhos J*, Chroni P, Samartzis A#, Datseris I. Nuclear Medicine, Radiology*, and Radiation Physics# Departments, "Evangelismos" Hospital, Athens, Greece.

AIM: PET/CT imaging has rapidly emerged, as an important imaging tool in oncology PET/CT imaging is an evolving technology in Greece, a country with no previous experience in dedicated PET-only systems. In this study we present an epidemiological survey for the first 2100 PET/CT cases in the largest (950 nursing beds) Greek public tertiary hospital ("Evangelismos" General Hospital), with a referral population of about 5 million.

MATERIALS-METHODS: We performed a retrospective review of the first 2100 patient's database, considering the indications and impact in patients' management, performed with a Discovery ST - GE HealthCare PET/CT scanner, from February 2007 to March 2009. The patient population consists of 1019 men and 1081 women (mean age 51 ± 13 years) referred exclusively for oncological indications. ¹⁸F DG was the unique radiotracer used.

RESULTS: Almost half of our daily practice included lymphoma and non small cell lung cancer-NSCLC patients (including Solitary Pulmonary Nodules-SPN evaluation): The main referrals for PET/CT examinations in patient percentages, were as follows: Hodgkin lymphoma (29%), Non-Hodgkin lymphoma (17,5%), Non Small Cell Lung Cancer (14%), Small Cell Lung Cancer (1%), Solitary Pulmonary Nodules (2,85%). Less frequent indications were: colorectal cancer (9%), breast cancer (7,1%), head-neck cancer (5,5%), testicular cancer (2,1%), cervical cancer (1,7%), kidney (1,5%), ovarian cancer (2%) and malignant melanoma (1%).

The following table summarizes the main indications of PET imaging studies, management alterations and their respective frequencies.

	Initial Staging	Restaging	Probable Recurrence	Therapy Evaluation	Down staged	Up staged
HL	6%	60%	19%	15%	32%	20%
NHL	6%	75%	14%	5%	28%	17%
NSLC	38%	26%	25%	8%	12.6%	37%
SCLC	19%	52%	26%		6.6%	53%
Colorectal cancer	2.5%	34%	54%	2%	11%	11%
Breast cancer	3%	31%	64%	1%	20%	18%
SPN	18FDG Positive		18FDG Negative		Upstaged	
	66%		34%		48%	

CONCLUSIONS: FDG-PET/CT seems to be a very useful method for oncology patient management, which was successfully incorporated in the Greek health-care system, due to its role in diagnosis, staging, restaging and treatment monitoring as well as radiation planning in patients with cancer. It provides patient comfort and high throughput as well as great diagnostic certainty and accuracy. The combination of functional/molecular and morphologic imaging has not only found its place, but is still gaining greater importance with new developments in technology and radiochemistry.

Breast Specific Gamma Imaging (bSgi) clinical use in France

Armelle Travade François Bouchet Alain Isnard centre d'imagerie médicale
république oncologie-radiothérapie PSR CIMROR Clermont Ferrand France.
Alain Cartron Olivier Rebillard SCINTIDOME médecine nucléaire Clermont
Ferrand France.
David Gray Agm Dillon 6800 ingeniering, France.

Sestamibi-based scintimammography has been known as a diagnostic imaging technique for Breast cancer detection since the early 1990s. However, only now is it rapidly gaining acceptance within the diagnostic imaging community, thanks mainly to the availability of new dedicated breast-imaging gamma cameras which enable Breast-Specific Gamma Imaging, or bSgi. The images produced by this technique are due to two different physiological mechanisms: the diffusion of the radioactive tracer throughout the circulatory system, further enhanced in the presence of neo-angiogenesis, and the intra-cellular binding of the tracer to each cell's mitochondria. The new Breast-specific gamma cameras take full advantage of the Sestamibi's action to deliver much improved sensitivity and positive predictive value, even for radiographic dense breasts. Studies carried out in the USA have confirmed the clinical efficacy of this bSgi technique in difficult cases where the mammography and ultrasound exams are unclear, or when looking for multifocal disease. The respective indications of Breast MRI and bSgi still require further fine-tuning, but it has been demonstrated that bSgi will generate fewer false positives than MRI and better detect non-invasive cancers (DCIS). Although the new Breast-specific imaging device is mobile and compact, its big advantage is the detector which adapts to the woman's morphology, mimicking all the views performed in standard mammography. This has the added bonus of allowing clinicians to easily correlate bSgi images with mammography and ultrasound images, thereby facilitating diagnostic interpretation, guided biopsy and pre-surgical planning. In cases where an unsuspected anomaly is discovered by MRI, a second-look ultrasound is further prescribed. bSgi's high specificity reduces these additional exams. Also, in certain cases, such as claustrophobia, obesity and ferromagnetic implants, bSgi can be prescribed as a direct replacement for Breast MRI.

Automatic Identification of Needle's Entrance Point and Angle in Vertebroplasty

S. Mardani Samani^{#1}, M. Yazdi^{#2}, M.H. Bagheri^{*3}

*[#]Department of Communications and Electronics, Faculty of Electrical and Computer Engineering,
Shiraz University, Shiraz, Iran*

¹mardanisamani@yahoo.com

²yazdi@shirazu.ac.ir

^{} Department of Radiology, Shiraz University of Medical Science, Shiraz, Iran*

³bagherimh@gmail.com

Abstract— Vertebral compression fracture (VCF) is a disease which affects the body of vertebrae usually due to osteoporosis or trauma. Vertebroplasty is a common therapeutic procedure to treat VCF. In Vertebroplasty, bone cement is injected into the body of fractured vertebra through the hollow needle via skin path. To do this, physicians insert the needle into the body experimentally guided by medical images. Proper and precise needle insertion is mandatory to avoid damage of sensitive structures such as spinal cord or nerve roots. In this paper, we propose an automatic approach to detect the needle's entrance point and its 3D direction using only the CT images of the patient. The results obtained by our approach have been validated by specialists and the approach can be used clinically

Keywords—Vertebral compression fracture, Vertebroplasty, CT images, Region Growing, morphological operation

Session IIc

Simultaneous analysis of myocardial perfusion SPECT and coronary CT angiography with a new integrated software: feasibility study.

C. Chauvet¹, F. Cachin¹, J. Lipiecki², D. Casset-Senon⁴, L. Cassagnes³, C. Thouly⁶, D. Alison⁵, A. Veyre¹, J. Maublant¹.

1. *J. Perrin Cancer Center, Nuclear Medicine, Clermont-Ferrand, France.*

2. *University Hospital, Cardiology, Clermont-Ferrand, France.*

3. *University Hospital, Radiology, Clermont-Ferrand, France.*

4. *University Hospital, Nuclear Medicine, Tours, France.*

5. *University Hospital, Radiology, Tours, France.*

6. *Segami Corporation, Columbia, MD, USA.*

Objectives: The fusion of coronary CT angiography (CTCA) with myocardial SPECT will permit to link anatomical lesions to functional defects. Mutual information could improve accuracy and prognostic value of myocardial perfusion SPECT and CTCA for detection of coronary artery (CA) disease. The aim of this study was to develop, on Oasis workstation ®, a software for 3D fusion of SPECT/CTA images, CA stenosis identification and perfusion SPECT quantification.

Methods: The original CTCA was first automatically masked to isolate the heart using mathematical morphological approaches. Thus lung vessels and bones were eliminated and a region of interest was defined around the heart for further processing. A top-hat method was used to remove large vascular structures from the heart and allow CA enhancement. CA were then segmented from a manually defined seed point using a region growing method based on a threshold (Hounsfield unit). If necessary, this threshold could be readjusted with a slider. After a standard manual CTCA reorientation, CA tree and perfusion SPECT were fused and displayed on a polar map and 3D object. CA stenosis was manually identified and CA post-lesion was highlighted in a relevant color. The software was tested on twelve patients, three healthy and nine with CA disease. Stenosis location was analyzed in comparison with myocardial SPECT defects.

Results: Automatic masking and CA segmentation (up to first branches) were successfully performed for each patient. Slider adjustment allowed optimizing CA segmentation even for low contrast enhancement. The CA tree superimposed with SPECT slices facilitated visual interpretation mainly for patients with faint perfusion abnormalities. The fused polar map and 3D object showed functional perfusion defects related to the corresponding stenosis location in patients with single vessel disease and more clinically useful with multi vessel disease. The different steps of the processing including segmentation and fusion were completed within two minutes.

Conclusions: We developed a software to extract the coronary artery tree from CTCA and fused it with myocardial SPECT. Fast processing made it particularly relevant for clinical practice. The integration of an automatic registration will provide a more accurate and reproducible image fusion. Providing combined information from myocardial perfusion SPECT and CTCA, this new integrated fusion software is useful for optimization of coronary artery disease diagnosis and cardiomyopathy.

ClearPEM-Sonic, a combined positron emission mammograph and ultrasound scanner

Benjamin Frisch^a, Etienne Auffray^a, Paul Lecoq^a

on behalf of the ClearPEM-Sonic consortium

^aCERN, Geneva, Switzerland

Breast cancer is one of the most frequent cancer types for women with an average life-time risk of about one eighth. As early detection leads to a very high cure rate, breast cancer screening is now a priority in healthcare policies of many countries. Conventional methods like X-ray mammography and echography show lesions but lack specificity. Additionally, those techniques are based on tissue density differences that complicate diagnosis in the case of dense breasts. The latter increases the number of false negatives. It is thus of highest importance to improve and provide additional means for early detection.

The Crystal Clear Collaboration developed a dedicated positron emission tomograph for mammography, the ClearPEM, as an addition to standard screening techniques. This device is based on LYSO:Ce crystals read out on both sides with avalanche photodiodes. This configuration allows measuring the depth of interaction in the crystals with a precision of two millimeters and thus contributes to good spatial resolution and high sensitivity. Initial trials with the first prototype installed at the Portuguese Institute of Oncology in Porto confirm a spatial resolution of 1.3 mm which is around 3-4 times better than conventional full-body PET.

For ClearPEM-Sonic, this performance is expected to improve as the light yield of the crystal matrices has been increased by 20% whilst keeping the same depth of interaction and energy resolution properties.

However, the main objective of ClearPEM-Sonic is to improve diagnosis by combining metabolic information gained with ClearPEM with morphological information from a new-generation ultrasonic transducer developed by SuperSonic Imagine. This novel transducer can also give objective information about tissue elasticity. ClearPEM-Sonic will then fuse metabolic, morphological and anatomical information to combine benefits from the specificities of both modalities.

The main challenge of combining both modalities is, aside from the mechanical integration, the proper fusion of both images to guarantee a mapping precision better than a millimeter. This has been solved by immobilizing the breast with an adapted contention system and providing best information about the position of both images in space via a combination of fiducial markers and high-precision positioning devices.

Development of anthropomorphic phantoms for combined PET-Ultrasound elastography breast imaging

DANG Jun ⁽¹⁾, Dachun Zhang^(1,3), Philippe Lasaygues⁽²⁾, S. Tavernier⁽¹⁾, Mingxi Wan⁽³⁾ and Serge Mensah⁽²⁾

1) Vrije Universiteit Brussel, Brussel, Belgium

1,3) Xi'an Jiaotong University, P.R. China

2) CNRS, Laboratory of Mechanics and Acoustics, Marseille, France

Abstract

As part of the development a combined PET-Ultrasound multimodal scanner for breast imaging by the Crystal Clear collaboration (The ClearPEM-Sonic project) we have developed and tested a phantom that can be used for making realistic images with both modalities.

In the first step we measured the propagation velocities of the acoustic waves, the attenuation coefficient and the elasticity (Young's modulus) for several series of different samples based on gelatine and agar mixtures. We determined which preparations reproduce the acoustical and elastic properties of different body tissues of interest in breast imaging such as fat tissue, glandular tissue, fibrous tissue and carcinomatous tissue.

In the Second step we have built phantoms where we added a small amount of FDG during the preparation of the phantom such as to give the different parts in the phantom activities similar to what is usually present in the breast during PET imaging. The phantom was then imaged on a Philips Gemini TF PET/CT and on a US scanner from ATL, HDI 5000. The images were superposed using rigid transformations to produce combined PET/US images.

We also evaluated the performance of our phantoms for US elastography imaging. Elastography is better for detecting the tumors than conventional US imaging. With elastography more clinical information can be obtained to help the clinical practitioner. We will test the combined ClearPEM/US scanner for its performance in mamographic imaging

Details on the procedure for producing the phantoms will be given.

**Evaluation of the positioning setup accuracy in prostate radiotherapy
using an a-Si flat panel portal imaging device.
The Aretaieion University Hospital experience**

M. Andreou, T. Gkatzis, C. Priskas, N. Christogiannis, M. Vergetidou, A. Trohana, C. Antypas, C. Armpilia, M. Balafouta, A. Zygoianni, P. Gkogkou, J Kouvaris, P. Sandilos and A. Gouliamos

Aretaieion University Hospital, Athens Medical School, Radiology department

Abstract

Introduction

Portal imaging is widely used in radiation therapy for patient setup (positioning) and treatment verification. Set-up errors, though undesirable are an inherent part of the radiation treatment process. They are defined as the difference between the actual and intended position with respect to radiation delivery. The experience, training and commitment of the radiation therapy staff as well as with the available time have a major impact on daily positioning accuracy.

Purpose

The aim of this study is to evaluate the 3-D random and systematic set-up errors for patients treated for prostate cancer by comparing DRRs (digitally reconstructed radiographs) with portal images taken from a Si-flat panel detector. In this way, efficiency and reproducibility of treatment can be confirmed.

Methods and Materials

43 patients with clinically prostate cancer have been treated with 3D-CRT (conformal radiation therapy) using a 6MV Siemens Oncor Impression linear accelerator. The linac is equipped with MLC (multi-leaf collimator) and a-Si flat panel detector (OPTIVUE 500 – 1024x1024) for portal imaging. All patients, during treatment, were immobilized with standard bi-lateral leg and knee immobilization positioners.

The set-up error is defined as the deviation between the actual and the expected patient position, normally calculated as a shift in the isocentric position when an image is compared against its corresponding reference, i.e.DRR.

Our dataset consists of DRRs and corresponding portal images on which 271 point positions were measured. The built-in image registration algorithm of the Siemens Coherence-Therapist workstation was used to calculate translational displacement in all patients Mean displacements, population systematic (Σ) and random (σ) errors, and 3D vector of displacement were calculated.

Results

The mean set-up errors in anterior-posterior (AP), medio-lateral (ML) and supero-inferior (SI) directions have been calculated -0.03cm, 0.18cm and -0.05 cm respectively. Population systematic (Σ) and random errors (σ) are 0.34, 0.27 and 0.34 cm and 0.25, 0.17 and 0.29cm in AP, ML and SI direction respectively.

Conclusion

Portal images with an a-Si flat panel detector in a 6MV linear accelerator was used to evaluate set-up errors for prostate cancer patients in our department. An overall set-up error of 2mm was calculated according to our analysis. This value was used to establish the internal margin due to patient position in the target delineation. Ranges of set-up errors are site specific and it is generally recommended that every radiotherapy department should generate data on its set-up accuracy without blindly adopting published margin recommendations.

UTILITY OF ADDITIONAL NECK 18FDG-PET/CT IMAGES IN PATIENTS WITH KNOWN OR SUSPECTED NECK MALIGNANCY

Giannopoulou C, Skoura E, Vlontzou E, Bournazos A, Chroni P, Skilakaki M*, Datsiris I
Nuclear Medicine and Radiology* Departments, "Evangelismos" Hospital, Athens, Greece.

AIM of our study was to evaluate the utility of additional neck-in-extension (NE) images in the workout of patients with known or suspected neck malignancy using 18FDG-PET/CT.

PATIENTS-METHODS: 78 patients 45 men, 33 women, mean age 64 (range 14-80) were examined with whole body 18FDG-PET/CT (WB) and additional NE images, in the time period January 2008- February 2009. Forty-three of them had lymphoma with neck involvement, 10 thyroid cancer, 8 had laryngeal cancer, 2 had nasopharyngeal cancer, 2 had tongue cancer, 2 salivary gland cancer and one had mandibular cancer. Of the rest 10 patients 4 had CUP, 2 came for melanoma staging and 4 had cervical node metastasis of a known primary cancer.

RESULTS: Of our 78 patients 36 (46%) had increased FDG neck uptake in the WB as well as in the additional NE image, and 25 (32%) had both tests negative. Of the rest 17 patients (22%) with inconclusive WB FDG-PET/CT the additional NE images revealed increased FDG uptake in 9 and absence of uptake in 8 patients.

CONCLUSION Additional NE images seem to be useful in patients with known or suspected neck malignancy and inconclusive 18FDG-PET/CT routine WB studies.

Some issues in Medical Imaging: State of the Art and Future Prospects

Andrew Todd-Pokropek
Dept. of Medical Physics and Bioengineering
University College London

Medical imaging has made enormous progress in the past decade, yet some important issues remain to be resolved. The first of these can be considered in terms of bandwidth, an example being MRI cardiac acquisition. We would like to push both (3D) spatial and temporal resolution. At the same time we would like to reduce the influence of disturbing effects such as (respiratory) motion. Similar issues exist in nuclear medicine, ultrasound and CT. Optimisation of sampling (intelligent acquisition) provides some solutions. A second major issue is that of partial volume, in order to include information at a finer scale than can be directly measured, by using techniques described as multi-scale modelling. A third major issue is that of extending the use of such imaging techniques to therapy, where image fusion, and image guided surgery are of great potential value. An overview of the current state of the art and potential for future progress will be presented in this exciting field of technology.

Session IIIa

Low-flux Imaging of Biomedical samples with Direct Detection CMOS Pixel Sensors in Low Energy Transmission Electron Microscopy

Marco Battaglia^{a,b,*}, Devis Contarato^b, Peter Denes^b,
Piero Giubilato^b, Velimir Radmilovic^b

^a*Department of Physics, University of California at Berkeley, CA 94720, USA*

^b*Lawrence Berkeley National Laboratory, Berkeley, CA 94720, USA*

Monolithic CMOS pixel sensors open new perspectives for fast nano-imaging through single electron direct detection in transmission electron microscopy (TEM). As the displacement damage threshold is proportional to \sqrt{E} , there is much interest in TEM at low energies, where recent advances in electron optics ensure deep sub-angstrom spatial resolution. This makes low energy TEM important for high resolution studies of biological samples. The multi-institutional TEAM (Transmission Electron Aberration-corrected Microscope) project is advancing Transmission Electron Microscopy (TEM) through improvements in electron optics, sample stages and detectors. The prototype TEAM instrument has demonstrated 50 pm spatial resolution in both TEM and scanning TEM. There are two main issues to be considered for imaging with low energy electrons. The first is the large fluctuations in the energy deposition. The second is the degradation of the point spread function (PSF) due to the increase of the electron multiple scattering in the detector. We present the results of a full characterisation of the TEAM 1k CMOS active pixel sensor (APS) at 80 keV on a TEAM project test column and a detailed comparison with **Geant-4** simulation. We demonstrate that with high-speed readout and single electron sensitivity afforded by CMOS APS detectors, there is a new imaging regime, which we call “cluster imaging”, where the electron flux is kept low enough that individual electrons can be observed and their position of impact reconstructed with much higher precision compared to the detector pixel pitch. The resulting PSF improves by a factor of 2-3 compared to that measured for bright field illumination. Cluster imaging thus appears particularly well suited for biological samples requiring low fluxes and low energy beam.

* Corresponding author

Email address: MBattaglia@lbl.gov (Marco Battaglia).

Silicon Photomultipliers, SiPM matrices and small animal PET

G. Llosá^{1*}, M. G. Bisogni^{2,3}, G. Collazuol^{2,3}, C. Lacasta¹, S. Marcatili^{2,3}, M. Melchiorri⁴,
C. Piemonte⁴, P. Barrillon⁵, S. Bondil-Blin⁵, C. de la Taille⁵, and A. Del Guerra^{2,3}.

¹Instituto de Física Corpuscular (IFIC, CSIC-UVEG), Valencia, Spain.

²University of Pisa, Department of Physics, Pisa, Italy.

³INFN – Pisa, Pisa, Italy.

⁴Center for Scientific and Technological Research, FBK-irst, Trento, Italy.

⁵Laboratoire de l'Accélérateur Linéaire LAL IN2P3-CNRS, Orsay, France.

Silicon photomultipliers have achieved the necessary level of development to be successfully employed in medical imaging applications. The use of such photodetectors in this field can offer significant advantages and improve the performance of the existing detectors. These devices are compact and robust, they have high gain, and their photon detection efficiency (PDE) is already higher than most PMTs. In addition, they are insensitive to magnetic fields.

The development of SiPM matrices that provide 2D position information has triggered the use of these photodetectors in medical imaging applications. Different manufacturers provide packages with 2D configurations of single elements, or develop monolithic arrays in order to minimize the dead area and thus maximize the PDE. Several groups are experimenting with this technology, in pixellated and continuous crystal configurations for PET detector heads, and for combined PET/MR technologies.

The University of Pisa and INFN Pisa are working in the development of a small animal PET tomograph that will exploit the benefits of this novel technology [1,2]. The PET detector head concept is based on continuous LYSO crystal slabs and silicon photomultipliers. The Center for Scientific and Technological Research, FBK- IRST (Trento, Italy) has developed monolithic matrices of 64 (8x8) pixel elements in a 1.5 mm x 1.5 mm pitch. The matrices have been tested with continuous LYSO crystals. The first tests result in an energy resolution of 15% FWHM at 511 keV, and a position resolution about 1 mm FWHM employing center-of-gravity algorithms. Ongoing tests aim at the improvement of the position determination with maximum likelihood algorithms. Results will be presented.

[1] Moehrs, S., et al., *A detector head design for small-animal PET with silicon photomultipliers (SiPM)*, Phys. Med. Biol. 51, 1113-1127, (2006).

[2] G. Llosá et al. *Energy, timing and position resolution studies with 16-pixel SiPM matrices for PET applications*. Accepted by IEEE Trans. Nucl. Sci.

* gabriela.llosa@ific.uv.es

A fast FPGA-based clustering algorithm for real time image processing

A. Annovi, M. Berretta, P. Laurelli

INFN, Laboratori Nazionali di Frascati, via E. Fermi 40, I-00044 Frascati (Roma), Italy.

P. Giannetti, G. Volpi, L. Sartori

INFN Sezione di Pisa, Largo Pontecorvo 3, 56127 Pisa, Italy

Abstract

Real time image analysis has undergone a rapid development in the last few years, due to the increasing computational power available at low cost. However computing power is still a limit for some high quality applications. High-resolution medical image processing, for example, are strongly demanding for both memory (~250 MB) and computational capabilities allowing for 3D processing in affordable time. The last few decades have actually seen revolution after revolution in the field of imaging; 3D and 4D imaging being the latest to join the bandwagon. Virtual endoscopy with 3D CT is now in the field for some time. The advent of newer xMATRIX technology in ultrasonography by Philips Healthcare now makes virtual endoscopy in its live volume imaging mode possible [1].

We propose the reduction of execution time of image processing exploiting the computing power of parallel arrays of Field Programmable Gate Arrays (FPGAs).

We apply this idea to an algorithm that finds clusters of contiguous pixels above a certain programmable threshold and process them to produce measurements that characterize their shape. It is a fast general-purpose algorithm for high-throughput clustering of data "with a two dimensional organization". The algorithm is designed to be implemented with FPGAs but it can also profit of cheaper custom electronics. The key feature is a very short processing time that scales linearly with the amount of data to be processed. This means that clustering can be performed in pipeline with the image acquisition, without suffering from combinatorial delays due to looping multiple times through the whole amount of data. The algorithm can be extended at 3-D images.

The algorithm is organized in two steps: the first step (core) clusters the data; the second step analyzes each cluster of data to extract the desired information. The second step can and should be tailored for each possible application. It is possible since these technologies combine the high performances of rigid dedicated hardware (capability of high parallelization) with most of the distinctive flexibility (reconfigurable logic) of general-purpose but lower-performance CPUs.

An additional advantage of this two steps approach is that the typical clustering related calculations (second step) are separated from the combinatorial complications of clustering. This separation simplifies the design of the second step and it enables it to perform sophisticated calculations achieving high quality in online applications. The algorithm is general purpose in the sense that only minimal assumptions on the kind of clustering to be performed are made.

It has been implemented into a XC5v1x155 [2] device and simulated. We report on timing performances.

[1]http://www.healthcare.philips.com/phpwc/main/shared/assets/documents/ultrasound/products/campaigns/pushing%20the%20boundaries/sonoscopy_whitepaper_iu22.pdf

[2]<http://www.xilinx.com/>

Session IIIb

Scatter correction in ^{201}Tl cardiac SPECT based on multiple energy windows data.

K Kacperski ¹⁾, K Erlandsson ²⁾, B F Hutton ²⁾

*The Maria Skłodowska-Curie Memorial Cancer Centre – Institute of Oncology, Warsaw, Poland ¹⁾;
Institute of Nuclear Medicine, UCL, London, UK ²⁾*

^{201}Tl is a tracer widely used in myocardial perfusion imaging due to its favourable physiological properties. However, due to the rather low energy of the main photopeak gamma photons the obtained images suffer from significant attenuation and scatter effects leading to reduced image quality.

The most efficient method of scatter correction is to include the accurate scatter model in the iterative tomographic reconstruction algorithm; however this is usually very computationally intensive and makes the reconstruction times excessively long. Another, much simpler approach known as Triple Energy Window (TEW) involves estimating the number of scattered photons in the photopeak window from the measurements of counts in narrow energy windows close to the main photopeak and subsequent subtraction from the main data.

We present a novel approach to scatter correction using projection data measured in multiple energy windows. Apart from the windows containing the photopeaks, counts in windows containing mainly scattered photons are measured. Based on measurements of thin rod sources, which involve virtually no in-object scatter, as well as anthropomorphic phantoms we developed an approximated model of the measured multiple window projections. The number of counts in each energy window is expressed as a linear combination of primary and scattered photons, accounting separately for in-patient scatter and detector/collimator effects. The model gives a set of linear equations which can be solved using the well known Maximum Likelihood Expectation Maximisation (ML-EM) algorithm. The solution is the estimated projection of the photopeak counts, from which the image can be reconstructed in the usual way. Contrary to the TEW method, the scatter windows we use are rather wide, and scatter-free estimates are obtained using the ML-EM algorithm, which takes into account the statistical nature of the data, therefore the noise in the resulting projections is significantly reduced.

The method has been implemented for D-SPECT system (Spectrum Dynamics, Israel) – a novel dedicated cardiac camera based on pixellated CdZnTe detectors. This kind of detectors involves additional specific effects, which have been included in the counts model. For anthropomorphic thorax phantom with myocardial perfusion defects we observed an improvement in a small lesion contrast by over 30%.

The method may be particularly useful when combined with the attenuation correction based on differential attenuation approach for multi-emission radionuclides, which requires accurate scatter pre-correction in order to work. The combined correction methods could provide accurate images from emission data only, without the need for extra transmission scan.

Calibration and Evaluation of a Dual Layer High Dynamic Range Display for Pathology Detection Tasks

Karl G. Baum, PhD¹ (Karl.Baum@rit.edu), Robert L. Harrigan¹, Natalie Tacconi¹, Jonathan B. Phillips², Rodney Heckaman, PhD², James A. Ferwerda, PhD², Kent M. Ogden, PhD³, María Helguera, PhD¹

¹Biomedical and Multimodal Medical Imaging Lab, Chester F. Carlson Center for Imaging Science, Rochester Institute of Technology, Rochester, New York

²Munsell Color Science Laboratory, Chester F. Carlson Center for Imaging Science, Rochester Institute of Technology, Rochester, New York

³Department of Radiology, Upstate Medical University, Syracuse, New York

Abstract: A two-alternative forced choice experiment was conducted to determine if diagnostic benefits exist when using high dynamic range displays for lesion detection tasks. The potential benefits resulting from both an increased dynamic range and an increased number of displayable just noticeable grayscale differences were evaluated. A custom high dynamic range display system was constructed using an LCD panel and DLP projector. The display, which provides a much larger contrast ratio than available with typical medical LCDs, was calibrated using the DICOM standard and its performance compared with that of an LCD.

Introduction: Liquid crystal displays (LCD) have replaced film as the display of choice in radiologic imaging. Use of LCD displays and associated digital images provide conveniences that film cannot, such as improved workflow efficiency and image enhancement options. However, film viewed over a light box in many cases still has a diagnostic advantage due to a larger dynamic range. Traditional light boxes have a peak brightness of around 4000 cd/m², providing a 3000:1 contrast ratio (maximum brightness divided by black offset) [Guarnieri]. This is well in excess of the 600-900 cd/m² and 600:1 contrast ratio of diagnostic LCD displays. For this reason it is believed that a display with an increased dynamic range and an increase in the number of perceivably different grey levels (just noticeable differences – JND) may provide diagnostic benefits. To evaluate this hypothesis, a custom high dynamic range (HDR) display was calibrated to the DICOM standard and two-alternative forced choice (2-AFC) studies were conducted to determine if the HDR display will provide an advantage for pathology detection.

Methods: A dual layer HDR display with a dynamic range of five orders of magnitude was investigated. The system includes a Plus U5-232 DLP projector (2000 Lumens, 2000:1 contrast ratio, XGA (1024 × 768) resolution, F = 2.6 – 2.9, F = 18.4 – 22mm) and an Apple 15" LCD panel with backlight removed (1024 × 768). The luminance channel of the projector is further modulated by the LCD panel, resulting in a bright display with a very low black level. The system includes a 150mm achromatic focusing lens, a Fresnel lens (custom Reflexite 24 inch), and a diffuser (Reflexite BP331), to focus and collimate the projector beam on the plane of the LCD panel.

A procedure for calibrating the display to the DICOM standard needed to be developed, as the additional dynamic range and quantization levels are achieved by controlling the display with two independent devices. Since the system luminance is multiplicative in nature, two characteristic curves, one for the projector and one for the LCD panel, were independently measured. Multiplying the two curves provides a two-dimensional characteristic surface. Given a desired luminance, this surface can be used to identify the appropriate digital driving levels for both the LCD panel and the projector in order to match the grayscale standard display function defined in the DICOM standard.

A two-alternative forced choice experiment following the methodology of [Ogden] was conducted to generate contrast detail curves representing a 92% correct detection rate. Several different display configurations were evaluated to determine if diagnostic benefits exist when using HDR displays for a lesion detection task.

Results and Conclusions: Calibration was successfully achieved. The display was found to have a low black level and a peak luminance of 1,800 cd/m², providing a 114,000:1 contrast ratio spanning 900 JNDs.

The HDR display was evaluated using multiple configurations: 1) using full dynamic range and all realizable JNDs, 2) using the full dynamic range and 256 DDL, 3) using the dynamic range of a standard diagnostic LCD and 256 DDL, 4) using the dynamic range of a standard diagnostic LCD and all realizable JNDs 5) using the maximum luminance of a standard diagnostic LCD but the lower black level of the HDR display and all realizable JNDs. The data from the study is currently being evaluated and will be presented.

Acknowledgements: This project was partially funded by a Kodak / CIS Innovated Research Grant.

Guarnieri, G., "Image Splitting Techniques for a Dual Layer High Dynamic Range LCD Display," IEEE Medical Imaging, 2008.

Ogden, K.M., "A Method for Analyzing Contrast-Detail Curves," IEEE Medical Imaging, 2007.

“Intelligent” CT: optimising image quality and reducing dose.

Selina Kolokytha¹, Lena Costaridou², Sofia Michopoulou¹, George Panayiotakis², Robert Speller¹

¹Univeristy College London, Dept. of Medical Physics and Bioengineering, London, UK

²University of Patras, Dept. of Medical Physics, Patras, Greece

Introduction:

Computed Tomography extends the clinical capabilities of X-ray imaging because of its high contrast sensitivity for visualizing tissues and the production of tomographic (slice) and 3D volumetric images. However, the dose associated to CT is significantly higher than that in radiography. Currently, a new generation of intelligent image sensors (I-ImaS) is proposed ^[1] aiming at optimisation of image quality, whilst minimising the radiation dose. This project aims to demonstrate the feasibility of adaptation of the I-ImaS technology to CT imaging, thus producing CT images of adequate quality by transmitting a lower overall dose to the patient.

Materials and Methods:

A homemade cylindrical phantom was utilised, mimicking a human wrist, and irradiated in a micro-CT system (Benchtop CT, X-Tek). Continuous CT acquisitions, of 720 views each, were made at increasing number of frames per view (corresponding to low, medium and high dose factors). The design of the “Intelligence” is based on the result of an image segmentation algorithm (k-means clustering ^[2]), which is applied to the sinogram of the view lines to identify tissue classes (bone, bone marrow and wax). The outcome of the segmentation algorithm is utilised to selectively replace pixels of projections corresponding to the tissue classes, with data corresponding to different classes. Subsequently, image quality is assessed by means of contrast to noise ratio (CNR) computed at three concentric regions of a rectangular ROI encompassing bone, bone marrow and its background.

Results and Discussion:

In Figure 1, CNR versus dose factor is plotted for the bone - bone marrow rings. The trendline indicates the relationship of CNR and dose for original acquisitions (low, medium and high dose). At the intermediate dose level, intelligently manipulated and reconstructed data can reach 97.4% the quality of the high dose image (having normalised the values taking the low dose as a minimum), by transmitting 25.3% of the total dose as compared to reconstructions of originally acquired data.

Conclusion:

This project proves the feasibility of the idea of an Intelligent CT, by “intelligently” manipulating sinogram data, and subsequently reconstructing images, which are of adequate quality but of significantly lower overall dose.

References:

^[1] <http://www.i-imas.ucl.ac.uk/>

^[2] Coleman GB, Andrews HC, "Image Segmentation by Clustering", Proc. IEEE 5, 1979, pp773-785.

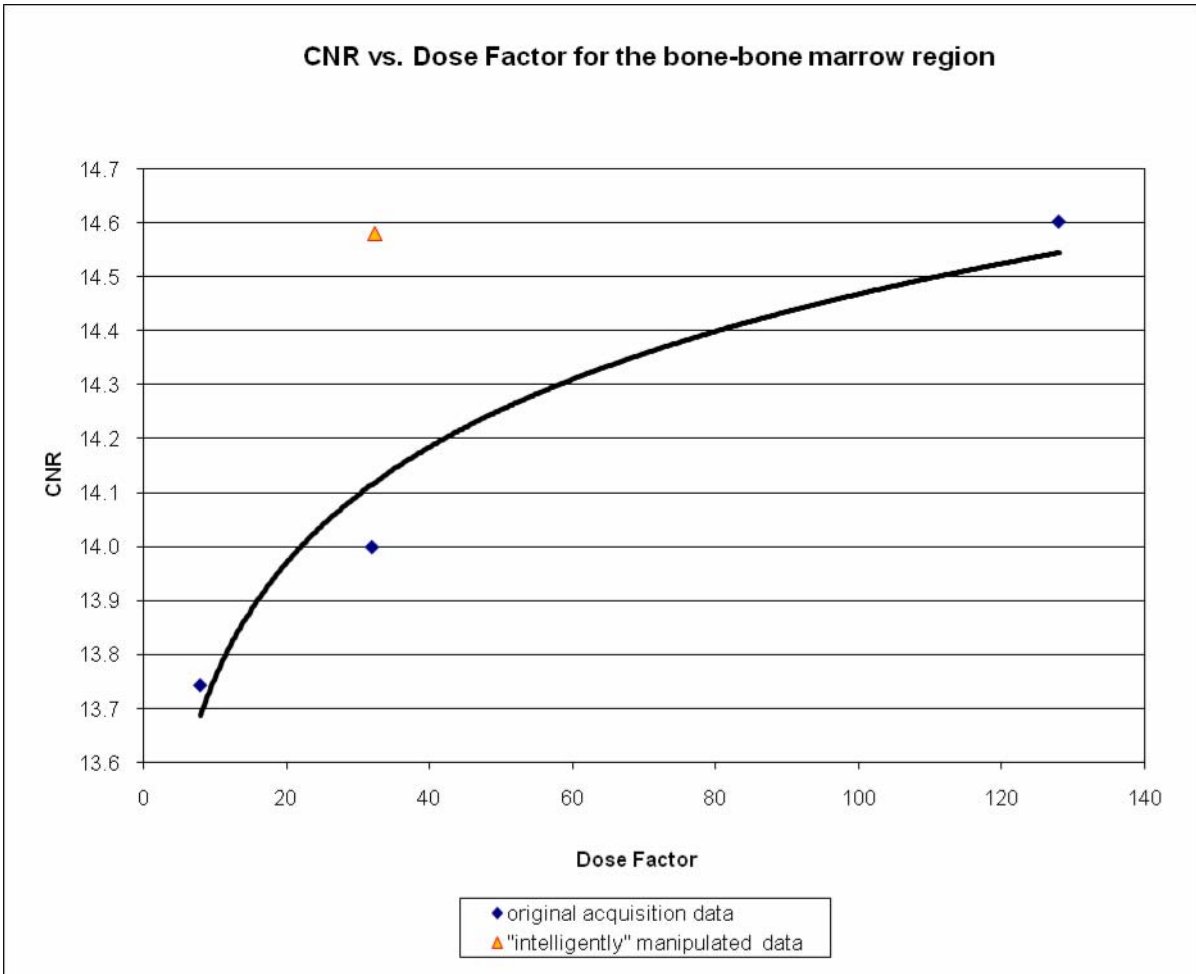


Figure 1: CNR and dose factor for original acquisitions (diamond symbols) and “intelligently” manipulated data (triangular symbol).

Intensity Inhomogeneity Correction in MRI of Lumbar Spine at 3T

Sofia Michopoulou¹, Lena Costaridou², Marianna Vlychou³, Elias Panagiotopoulos⁴, Robert Speller¹, George Panayiotakis², Andrew Todd-Pokropek¹

¹University College London, Dept. of Medical Physics and Bioengineering, London, UK

²University of Patras, Dept. of Medical Physics, Patras, Greece

³University of Thessaly, Dept. of Radiology, Larisa, Greece

⁴University of Patras, Dept. of Orthopaedics, Patras, Greece

Introduction: MRI intensity inhomogeneity is a smooth variation (10%-20%) in image intensity attributed to RF non-uniformity and patient anatomy, and is more prominent when surface coils and high magnetic field MR scanners are used. Intensity inhomogeneity can adversely affect the performance of automated image analysis techniques^[1] and particularly segmentation techniques that assume homogeneity of intensity within each tissue class^[2]. In lumbar spine imaging, MRI is the modality of preference for evaluating degenerative alterations. In this study, we work towards the correction of intensity inhomogeneity in MR images of the lumbar spine acquired by a 3T scanner, testing three different methods.

Methods: The inhomogeneity correction methods tested are: (a) homeomorphic filtering for removal of low frequency image content, (b) entropy minimization of image information content, and (c) nonparametric nonuniform intensity normalization^[2] (N3) maximizing the high frequency content of images. Processing was carried out using the MATLAB and MIPAV softwares. A case sample of 5 lumbar spine T2-weighted mid-sagittal MR images acquired by 3T Signa GE MR scanner using an HDCTL surface coil was used for evaluating the inhomogeneity correction methods. Direct evaluation was carried out by calculating of the coefficient of joint variation (CJV), which is an estimate of intensity values overlap between two image tissue classes^[1] (i.e. in 25 pairs of vertebral bodies and intervertebral discs). Moreover, indirect evaluation^[1] was performed by testing the effect of inhomogeneity correction on the accuracy of intervertebral disc segmentation^[3].

Results and Discussion: The coefficient of joint variation was found to be lower in spine images corrected for intensity inhomogeneity, in comparison to the uncorrected ones, for all three methods tested ($CJV_{\text{uncorrected}}=0.774$, $CJV_{\text{homeomorphic}}=0.760$, $CJV_{\text{entropy}}=0.773$, $CJV_{\text{N3}}=0.760$). This indicated that all three correction methods resulted in reduced intensity inhomogeneity and improved separability between bone and disc tissue. In addition, intervertebral disc segmentation accuracy (as measured by the Dice Similarity Index) was improved when intensity inhomogeneity correction was applied as a preprocessing step to image segmentation for the homeomorphic filtering and N3 methods ($\text{Dice}_{\text{uncorrected}}=92.3$, $\text{Dice}_{\text{homeomorphic}}=92.6$, $\text{Dice}_{\text{entropy}}=92.3$, $\text{Dice}_{\text{N3}}=93.2$). The N3 method provided the best overall performance, and resulted in statistically significant improvement of intervertebral disc segmentation accuracy ($P<0.001$), as compared to uncorrected data.

Conclusion: This study demonstrated the strong potential of the N3 method in correcting intensity inhomogeneity of lumbar spine MR images at 3T, and improving the performance of the automated disc segmentation method.

[1] U. Vovk, F. Pernus and B. Likar, "A Review of Methods for Correction of Intensity Inhomogeneity in MRI", IEEE Transactions On Medical Imaging, Vol. 26, No. 3, March 2007.

[2] J. Sled, A. Zijdenbos and A. Evans, "A Nonparametric Method for Automatic Correction Of Intensity Nonuniformity in MRI Data", IEEE Transactions On Medical Imaging, Vol. 17, No. 1, February 1998.

[3] S. Michopoulou, L. Costaridou, E. Panagiotopoulos, R. Speller, G. Panayiotakis, and A. Todd-Pokropek, "Atlas-Based Segmentation of Degenerated Lumbar Intervertebral Discs From MR Images of the Spine", IEEE Transactions On Biomedical Engineering, in press, DOI: 10.1109/TBME.2009.2019765.

¹s.michopoulou@ucl.ac.uk

²a.todd@ucl.ac.uk

Session IVa

Advances in Phase Contrast Imaging

Alessandro Olivo

Department of Medical Physics and Bioengineering, UCL, London WC1E 6BT, UK

X-ray Phase Contrast imaging (XPCi) has been the hottest topic in x-ray imaging over the last decade. Three different methods were developed at Synchrotron Radiation (SR) facilities, and they were all demonstrated to provide striking improvements over conventional, absorption-based x-ray imaging. XPCi is based on a different physical principle (refraction and/or interference), which substantially increases the visibility of all details and allows the visualization of features previously considered undetectable. The only downside – albeit not a minor one – is that up to a few years ago it looked like XPCi was only possible at SR facilities.

In terms of transferability to real world applications, and to medical applications in particular, two of the three techniques mentioned above were ruled out almost immediately because they are based on perfect crystals: Bonse/Hart interferometry and analyzer-based/diffraction-enhanced imaging. Perfect crystals require the x-ray beam to be parallel and monochromatic, which is hardly achievable outside SR facilities unless by reducing the available x-ray flux by several orders of magnitude.

Researchers therefore focused on the third approach – free-space propagation XPCi, which does not require optical elements between sample and detector. However, in this case image quality is severely affected by the dimensions of the focal spot. This means that good image quality can be obtained by means of microfocal sources, but these do not provide sufficient output for medical applications. As soon as the focal spot is made big enough to allow exposure times compatible with clinical practice, there is almost no improvement in terms of image quality over conventional absorption imaging.

More recently some expectation was raised by a technique based on the Talbot/Lau (or grating) interferometer. A third grating is added to the two forming the classic Talbot interferometer, with the role of chopping an incoherent source into mutually incoherent, but individually coherent slices. XPCi images with an extended source were obtained in this way, but again at the price of an excessively increased exposure time as the third grating strongly suppresses the source output.

Finally, a new method based on coded apertures was recently developed at UCL. In this case, two sets of coded aperture with a 50% fill-factor are placed at either side of the imaged object, to make sure that only the portions of the beam actively contributing to the XPCi signal contribute to image formation, thus maximizing the signal itself while suppressing any unwanted background. This method was demonstrated to work with fully divergent, fully polychromatic beams produced by a conventional source with a focal spot as big as 100 μm , i.e. fully compatible with state-of-the-art mammography sources. As the 50% fill-factor of the coded apertures only imposes an increase in exposure time of a factor of ~ 2 , this method currently seems the most promising in terms of enabling an effective transfer of XPCi into clinical practice.

Measuring Trabecular Bone Orientation by Diffusion Tensor Imaging

Bailiang Chen^{a,1}, Pierre-Andre Vuissoz^{b,c,2}, Amaka Offiah^{d,3}, Martin Fry^{a,1}, Andrew Todd-Pokropek^{a,4}

^aDepartment of Medical Physics and Bioengineering, University College London, Malet Place Engineering Building, Gower Street, London, WC1E 6BT, UK; ^bIADI, Nancy-Université, Nancy, France; ^cINSERM, U947, Nancy, France; ^dGreat Ormond Street Hospital for Children, Great Ormond Street, London, WC1N 3JH, UK

Motivation: Diffusion tensor imaging (DTI) provides an important insight into tissue structure at the cellular level by measuring the translational displacements of particles. Though actively used in brain research, diffusion-based techniques have also been extended to the musculoskeletal system, but mainly *ex vivo* or only using diffusion-weighted imaging. DTI has the power to determine bone status by characterizing the micro-structure of trabecular bone network through restricted diffusion, but is rarely exploited [1]. Trabecular bone can be considered as a typical porous media system [1] where diffusion MR is widely used to measure porosity and orientation [2]. Here, we present the preliminary results of our *in vivo* studies applying DTI to human tibia and the technique's ability to reveal trabecular network orientation at the micro-scale by reconstructing diffusion tensors and tracking the dominate diffusion directions.

Methods: The right knee of a 46 year-old male with no record of any knee disorder was scanned on a 3T GE SIGNA system with a diffusion-weighted pulse sequence (PGSE preparation with EPI read-out). One non-diffusion-weighted dataset (b -value = 0 s/mm²) was acquired (Fig. 1a). 35 uniformly distributed (on a unit sphere) diffusion directions were then applied with b -value = 400 s/mm². An 8-channel knee-coil was placed over part of the knee joint and upper tibia. The acquisition matrix was 128×128 and was interpolated to 256×256, with in-plane resolution 0.89×0.89 mm, and slice thickness 4 mm. T₁-weighted images (2D fast spin echo, 0.31×0.31 mm in-plane resolution, 512×512 acquisition matrix) were also acquired to show the anatomical correspondence (Fig. 1c). The diffusion tensor in each voxel was reconstructed by fitting the log-measurement to the Gaussian displacement model by linear regression. A background threshold is chosen to mask out noise before the fitting procedure. Fractional anisotropy (FA) (Fig. 2a) and the principle diffusion directions were calculated based on the computed tensors (Fig. 2b). A region of interest was chosen inside the trabecular bone, and the coherence of the orientation of diffusion was calculated using a fibre tracking algorithm developed for brain diffusion imaging. All the analyses were performed with CAMINO [3] and MATLAB (R2008a). Noise was assessed by comparing standard deviations of intensity in defined ROIs (9×9 neighbourhood) at background and bone region respectively.

Results:

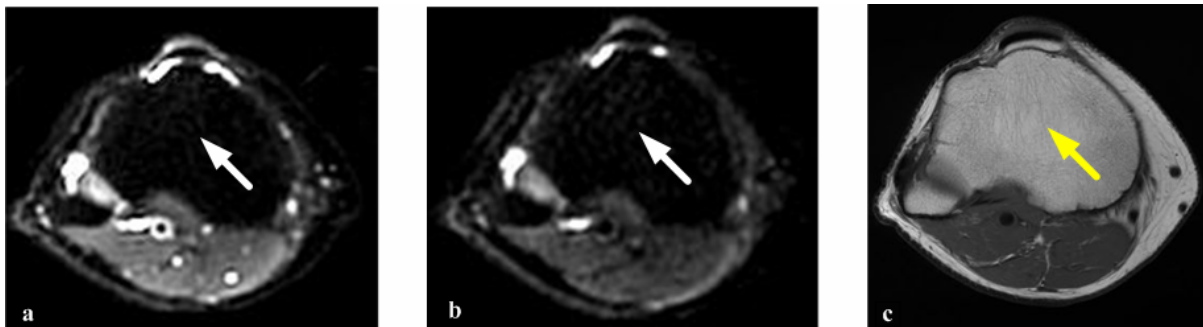


Fig. 1: a) $b = 0$, b) $b = 400$ s/mm², images showing visible intensity change corresponding to the trabecular bone patterns clearly visualized by the T₁ image in c) (arrow).

The data acquired are shown in Fig. 1a and 1b. Contrast decrease was revealed in both the region of trabecular bone and muscles when diffusion gradients were applied. Calculated bone ROI standard deviation is 34, three times higher than in the noise ROI's 11.39. FA maps and Eigen systems of the diffusion tensors were computed and are shown in Fig. 2a and 2b. The orientation of the trabecular bone network is shown in Fig. 2c, indicating the anisotropic behaviour of particles during the DTI pulse sequence.

Conclusion and Future Work: We have shown here the feasibility of applying DTI to the tibia *in vivo* and its ability to extract trabecular bony orientation, which is determined by the functional adaptation of bone [4]. Ongoing work is to improve the protocol to increase the SNR, and relate this to the principal directions of the stress tensors.

Acknowledgements: This work is partly funded by the EU project MRTN-CT-2006-035763 '3D anatomical human'.

References: 1. Capuani et al. (2005) Solid State Nucl Mag, 28:2-4, 266-272; 2. Wong, Po-zen (1999), Methods of Physics of Porous Media; 3. <http://www.cs.ucl.ac.uk/research/medic/camino/> 4. Cowin, S.C J. (1986) Biomech. Eng. 108: 83-88

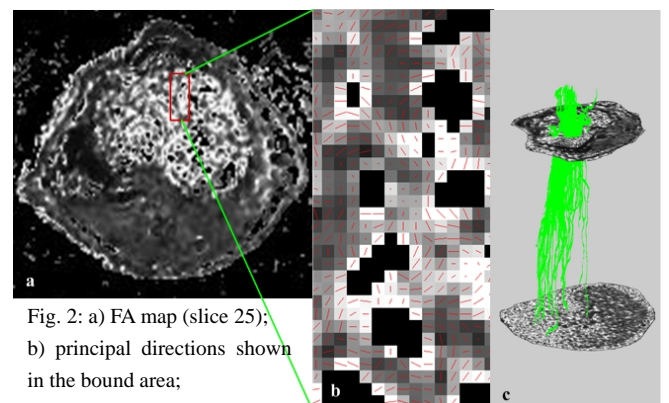


Fig. 2: a) FA map (slice 25); b) principal directions shown in the bound area; c) structure orientation found by following principal directions of diffusion tensors.

¹ {bchen, mefry}@medphys.ucl.ac.uk ² pa.vuissoz@chu-nancy.fr ³ amaka.offiah@nhs.net ⁴ a.todd@ucl.ac.uk

Reconstruction Optimization for γ -Camera Planar Images from Resistive Chain Readouts

D. Thanasas¹, D. Maintas², E. Georgiou⁴, N. Giokaris^{1,3}, A. Karabarbounis^{1,3}, M. Mikeli¹,
C.N. Papanicolas^{1,3}, L. Ragkousis¹ and E. Stiliaris^{1,3*}

¹Department of Physics, University of Athens, Athens, GREECE

²Institute of Isotopic Studies, Athens, GREECE

³Institute of Accelerating Systems & Applications (IASA), Athens, GREECE

⁴Medical School, University of Athens, Athens, GREECE

Abstract

The charge limitation for peripheral FOV events detected by the most commonly used Position Sensitive Photomultiplier Tubes (PSPMTs) results to spatial distortions and non-uniformities of the obtained planar images. These effects can be corrected with newly developed sophisticated techniques operating on the charge signals from the individual wires of the multi-anode systems. However, a similar algorithmic approach for the simple case, where the resistive chain readout technique is used and, consequently, the original charge distribution information is lost, is not applicable. In this work the development of a new method to eliminate these distortion effects in the planar images for Gamma-Camera systems based on resistive chain techniques is presented. The proposed model, which incorporates an *a priori* knowledge of three parameters related to light diffusion inside the scintillation crystal in use, provides an accurate, analytically calculated estimate of the spatial correction as a function of the primary reconstructed planar position from the resistive chain signals. This algorithm can be used online on an event-by-event basis and can be applied to both, homogeneous and pixelated crystals. Experimental results for simple phantoms and various CsI(Tl) crystals with different thickness are presented.

Summary

According to the resistive chain readout, the primary planar position information (X_{res}, Y_{res}) is simply reconstructed from the end-signal difference due to the charge division technique (Fig.1). The proposed model provides the correction estimates in terms of the quantities dX and dY , which can be analytically calculated as a function of the primary information (X_{res}, Y_{res}). No lookup tables or other interpolation techniques based on preceding calibration data [1] are used.

The light distribution on the detective surface of the PSPMT is assumed to be described by the general expression [2]:

$$G(P_x, P_y, x, y) = A_1 \exp\left[-\frac{(x - P_x)^2 + (y - P_y)^2}{2\sigma_1^2}\right] + A_2 \exp\left[-\frac{(x - P_x)^2 + (y - P_y)^2}{2\sigma_2^2}\right],$$

where (P_x, P_y) denotes the position of the detected gamma ray inside the scintillation crystal. The charge accumulated by the multi-anode wires with a constant amplification factor k (Fig.2, left) can be calculated by integrating accordingly the previous relation:

$$Qx_i = k \int_{y1}^{y2} G(P_x, P_y, x_i, y) dy \quad (\text{x-direction}) \quad \text{and} \quad Qy_i = k \int_{x1}^{x2} G(P_x, P_y, x, y_i) dx \quad (\text{y-direction}).$$

Finally, the resistive chain signals are calculated by proportionally adding the contribution from each of the above estimated N individual wire charges. For the x-direction the signals are:

$$X_A = \frac{N}{N+1} Qx_1 + \frac{N-1}{N+1} Qx_2 + \dots + \frac{1}{N+1} Qx_N \quad \text{and} \quad X_B = \frac{1}{N+1} Qx_1 + \frac{2}{N+1} Qx_2 + \dots + \frac{N}{N+1} Qx_N,$$

and also similarly for the y-direction. It is obvious, that the required corrections $dX = P_x - X_{res}$ and $dY = P_y - Y_{res}$ depend on the light diffusion parameters $(A_1/A_2, \sigma_1, \sigma_2)$ (Fig.2, right). This set of

* This work is partially supported by the 03EΔ287 research project, implemented within the framework of the "Reinforcement Program of Human Research Manpower" (PENED) and co-financed by National and Community Funds (25% from the Greek Ministry of Development-General Secretariat of Research and Technology and 75% from E.U.-European Social Fund).

parameters is characteristic for each type of scintillation crystal and the gamma energy of the radio-tracer in use.

Figure 1

Readout system based on the resistive chain technique. The reconstructed planar coordinates X_{res} and Y_{res} are corrected by the quantities dX and dY respectively to eliminate the distortion effects due to deficient charge detection.

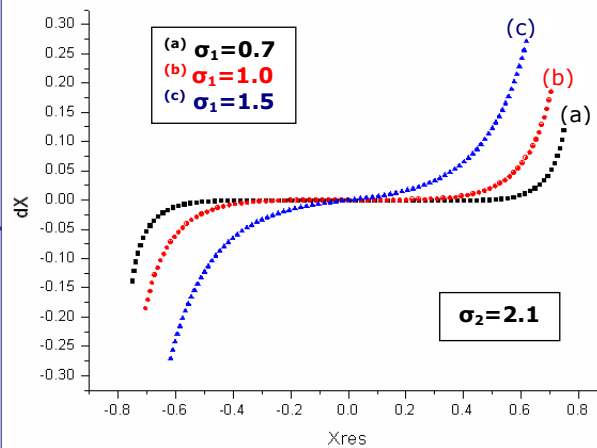
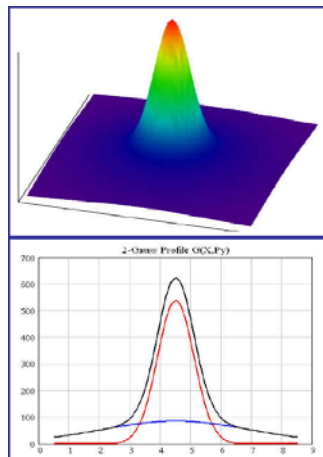
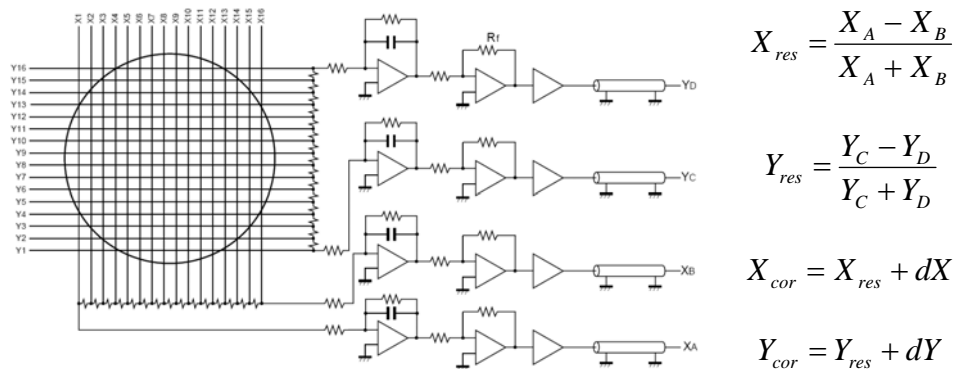
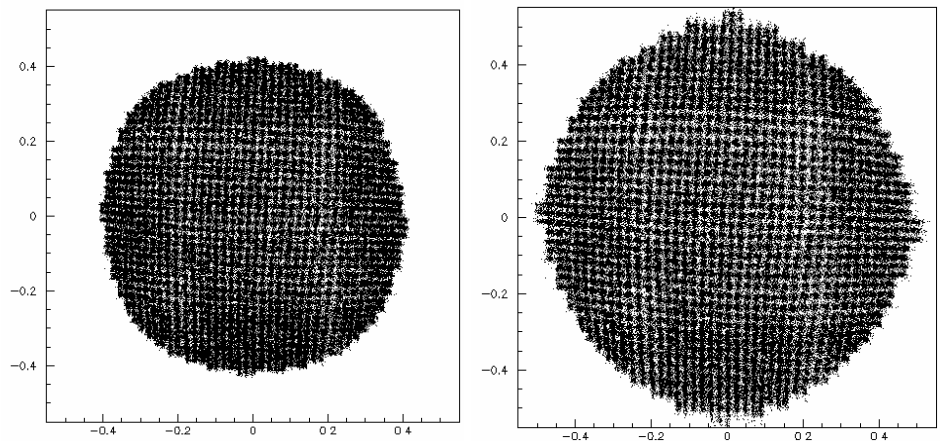


Figure 2

Left: Modelled light distribution $G(P_x, P_y, \sigma_1, \sigma_2)$ on the detective surface of the position sensitive photomultiplier tube and the resulting accumulated charge along to the projection axis. **Right:** Calculated correction $dX(X_{res})$ for the horizontal axis based on the presented model for various values of the parameter σ_1 . Similar correction applies also to the y-axis. As expected, corrections are negligible at the central FOV region and show an increasing effect approaching the field edges.

Figure 3

Planar image of a uniform ^{60}Co test source obtained with the γ -Camera system equipped with the R2486-05 PSPMT and a 3mm CsI (TI) pixelated scintillation crystal without collimation. The uncorrected (X_{res}, Y_{res}) image is shown on the left, the corrected (X_{cor}, Y_{cor}) on the right.



In this work, a small field, high resolution γ -Camera system based on the R2486-05 PSPMT from HAMAMATSU is used. A typical application of the analytical correction algorithm on an event-by-event basis is shown in Fig.3. Several other experimental results for simple phantoms and various CsI(Tl) crystals with different thickness are presented. Direct comparison of the parameter sets $(A_1/A_2, \sigma_1, \sigma_2)$ used in each crystal geometry with expected values from optical photon simulation (DETECT2000) is also given.

References

[1] D. Thanasis *et al.*, "Correcting Spatial Distortion and non-Uniformity in Planar Images from γ -Camera Systems", *IEEE Nuclear Science Symposium Conference Record M06-19*, pp. 3711-3714, 2008.
 [2] M. Mikeli *et al.*, "A New Position Reconstruction Method for Position Sensitive Photomultipliers", *IEEE Nuclear Science Symposium Conference Record M10-104*, pp. 4736-4741, 2008.

Accelerated Image Reconstruction on a Cluster of Two AMD GPUs in CBCT with Non-uniform Detector Geometry

A. Bonissent, C. Morel

Centre de Physique des Particules de Marseille (CPPM), IN2P3/CNRS and Université de la Méditerranée Aix-Marseille II, France

ABSTRACT

The imXgam group of CPPM has developed the XPAD3 hybrid pixel X-ray detector with 560x960 pixels (130 μm each). A Cone Beam CT scanner (CBCT) has been built, based on XPAD3 detectors, which enables volume reconstruction of a complete mouse with 65 μm resolution. However the basic unit is a chip whose width is about 1cm. These are assembled into barrettes which are in turn assembled in a tiled structure in order to reduce the dead regions. This results in a geometry where the apparent position and size of the pixels are not uniform. The volume reconstruction is performed using the analytic method of Feldkamp, Davis and Kress. Reconstruction time was estimated to a few hours due to the large number of pixels and images and the added complexity of the interpolation resulting from the non-uniform geometry. The algorithm was ported to a GPU architecture based on the AMD Firestream9270 board driven via the Brook+ library. All the processing is performed in the GPU and the host CPU is used only for steering and I/O operations. For improved performance, a dual-GPU version has been developed. With this setup, the total reconstruction time is of order 2 minutes, mostly limited by disk I/O. Compared to the usual CPU implementation the gain in speed is of the order of 100.

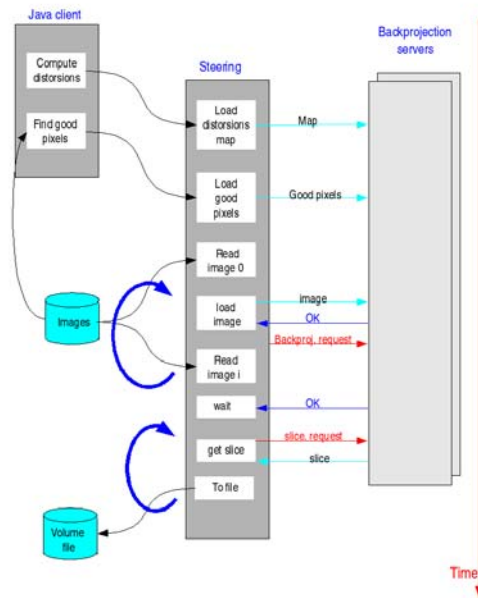


Figure 1 : the multi-GPU architecture

Fuzzy linear regression approach for estimation of photon escape probability from HPGe detectors

Farshid Babapour Mofrad, Dariush Sardari, Ali Abbaspour

Faculty of Engineering, Science and Research Branch, Islamic Azad University, Tehran, Iran

Farshid.mofrad@yahoo.com

Photon escape probability is important in the formation of single escape and double escape peaks in gamma ray spectrum[1]. Due to remarkable variation in detector sensitive volume and uncertainty in spectroscopic data, fuzzy regression is suggested to provide a general relationship between detector volume and 511keV photon escape from HPGe detector. Fuzzy least square method [2] (FLSM) is applied and implemented to experimental escape data [1]. Regression coefficients are found and deviation of results for model obtained.

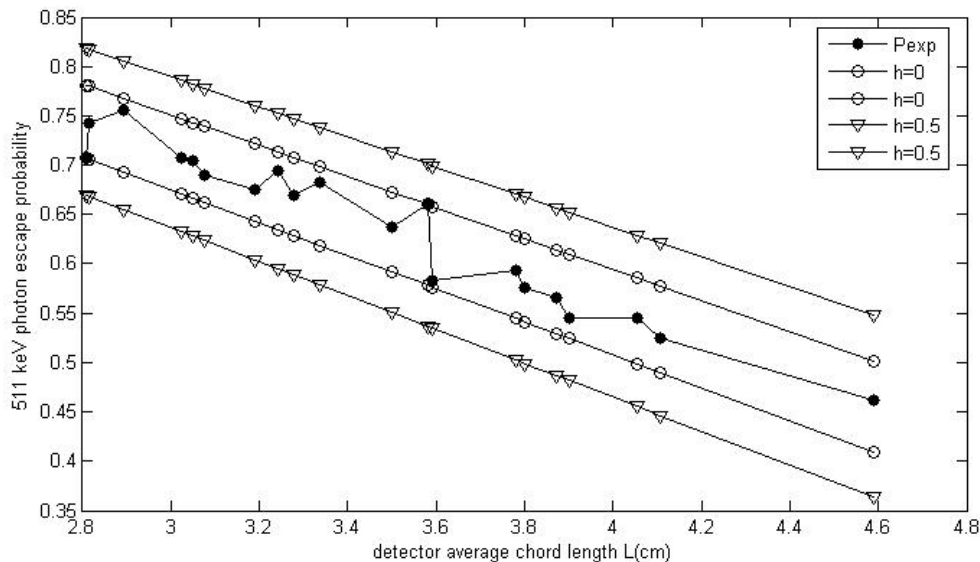


Fig. 1 graph of fuzzy regression for escape data in two $h=0$, $h=0.5$

The term h is referred to as a measure of goodness of fit or a measure of compatibility between data and a regression model. The data from fitted curve to the escape data are used as the crisp input to our computation program and the fuzzy output is compared to the result of FLSM results.

Keywords: Fuzzy regression; HPGe detector; Photon escape probability.

References

[1] Sardari D, Baghini NM, 2005. Escape probability of 511 keV annihilation photon from HPGe detectors. Radiation Measurements. 39, 387-390.

[2] Ming M, Friedman M, Kandel A, 1997. General fuzzy least squares. Fuzzy Sets and Systems 88, 107-118.

Session IVb

JEAN MAUBLANT MAMMOGRAPHY SESSION AT ITBS 2009 MILOS (TBC)

WHITE REPORT ON MULTIMODALITY IMAGING IN EARLY BREAST CANCER DETECTION. MOLECULAR IMAGING BROADENS EUROPEAN SCOPE IN BREAST IMAGING. Patrick N. Guiderdoni Claude Bernard School of Medicine Lyon Est France. Editorialist at net&com medicine publishing Agency. Review of literature and survey at Pôle Santé République Clermont Ferrand France CIMROR Radiology Unit of Alain Isnard and al. To date, mammography remains the only breast imaging technique that prospective trials have shown to reduce mortality from breast cancer. However, results from studies, using gamma camera technology to image the breast suggest that it can effectively detect cancers that are not found on mammograms or by clinical exam, and may be even prove to be superior to MRI for detecting breast lesions. The technique, commonly referred in the US studies to as breast – specific- gamma –imaging (bSgi) , and introduced last June 2008 in Europe, uses a high resolution small field-of-view gamma camera can detect early stage cancer (as small as 3 mm), identify lesions independent of tissue density en provide multiple angle view for direct correlation to mammograms : cooperation between nuclear practitioners keen on capture images of the metabolic activity of breast lesions on biology and pathophysiology basis through radiotracer , and clinical radiology with a greater focus and expertise on the demonstration of anatomy and pathology. Research in the field of imaging is now a multidisciplinary process with radiologists and nuclear medicine specialist working not only with clinicians from other disciplines but also with physicist, biochemists, physiologists, computer experts and bioengineers. The specialties must review their relationship to maximize the forecast of technical advances and maximise patient benefit and technical progress.

Characterization of cardiac action potential propagation in pathologic hearts using optical imaging, MRI and computer modelling

M. Pop¹, J. Relan², M. Sermesant^{2,3}, A. Soong¹, T. Mansi², G. Liu¹, Paul Fefer¹,
A.J. Dick¹, E. Crystal¹, E.R. McVeigh⁴, H. Delingette², N. Ayache², G.A. Wright¹

¹ Sunnybrook Health Sciences Centre, University of Toronto, Canada; ²INRIA, ASCLEPIOS project, Sophia Antipolis, France;

³Division of Imaging Science, King's College, London, UK; and ⁴Johns Hopkins University, Baltimore, Maryland, USA

BACKGROUND: Arrhythmia associated with myocardial infarct is the main cause of sudden cardiac death, accounting for > 400,000 deaths annually in USA [1]. Computer modelling can help us understand and predict the propagation of action potential (AP) in healthy or abnormal hearts. Such models can be integrated in clinical diagnosis and therapy planning [2]. Image-based theoretical models are available to explore the electrophysiology of small hearts, but lack experimental validation [3]. We have developed a 3D MR image-based model and experimentally validated it (using optical imaging and MRI) in large, healthy swine hearts [4]. However, before translating our computer model into clinical applications, we need to validate model's predictions in pathologic hearts, which is the purpose of the current work.

METHODS: Optical fluorescence imaging using voltage-sensitive dye (di-4-ANEPPS) was performed in 6 pathologic porcine hearts (with either chronic infarct >4week, or acute myocardial lesions generated via RF ablation) attached to a Langendorff perfusion system (Fig.1a). Both type of scars were electrically unexcitable, thus did not propagate AP. The cardiac propagation of AP was mapped with 3.7ms temporal and 0.7mm spatial resolution (Fig1b) using MiCAM02 cameras (BrainVision, Japan), as described in [4]. Maps of isochrones (lines of identical activation time) were computed from the measured AP waves. Two hearts (one infarcted and one with RF lesion) were further imaged using a 1.5T MRI scanner and a diffusion-tensor sequence, for anatomy and fiber directions (0.4x0.4x2mm voxel size). The MR images were then segmented into zones (healthy/scars) using image thresholding and clustering methods. Next, a 3D volumetric mesh was generated from the MRI of the heart anatomy and the fiber directions were specified at each node in the mesh. We used macroscopic reaction-diffusion equations to solve for action potential, see [5] for details. An important input parameter in the mathematical model is the electrical conductivity "d"; thus, specific values for "d" were assigned per different segmented zones of the mesh (e.g. zero in the scar). The output of the mathematical model is the AP wave, from which we computed theoretical isochrones and compared them to the measured isochrones. From isochronal maps we also estimated the conduction velocity of AP wave (which is known to vary with the square root of parameter "d"). The comparison between the measured and theoretical isochrones allowed us to calibrate and iteratively adjust model's input parameters (i.e., specifically, we adjusted the conductivity maps).

RESULTS: Figs 1 (c and d) show an MR image (long-axis of the heart) and corresponding segmented zones (healthy, dense scar and peri-infarct). Histopathology (using Masson Trichrome stain) confirmed the presence of heterogeneous infarct and was in good agreement with segmentation results and with corresponding areas of no AP propagation. A snapshot of a magnified area between the right ventricle and septum shows a dense collagenous scar, with a peri-infarct zone comprised of islands of surviving bundles (Fig 1e). A simulated isochronal map for this heart is shown in Fig. 2a; a map of parameter "d" after adjustment is shown in Fig 2b. The mean absolute error in depolarization time between experiment and simulations was 56ms before the adjustment; after an iterative adjustment the error decreased to 6ms (Fig. 2c). For the heart with RF lesion (not shown), the error decreased from 57ms to 9.2ms.

CONCLUSION: Validation of cardiac predictive models is an important step prior their integration into clinical applications. Here, we demonstrated the feasibility of calibration and adjustment procedures of an image-based model in pathologic hearts (with unexcitable scars) using optical and MRI data. Similar steps will be required to improve the accuracy of theoretical predictions in patient-specific models.

Reference: [1] Huikuri HV *et al* 2001 N Engl J Med 345:1473-1482; [2] Clayton RH and Panfilov AV 2008 Prog Biophys Mol Biol 96(1-3): 19-43; [3] Vadakkumpadan *et al* J. Electrocardiol 2009 42(2)157, e1-10; [4] M. Pop *et al* Med. Imag. Analysis 2009 Apr;13(2):370-80; [5] Sermesant *et al* 2006 IEEE Tran Med Imag 25(5) 612-625.

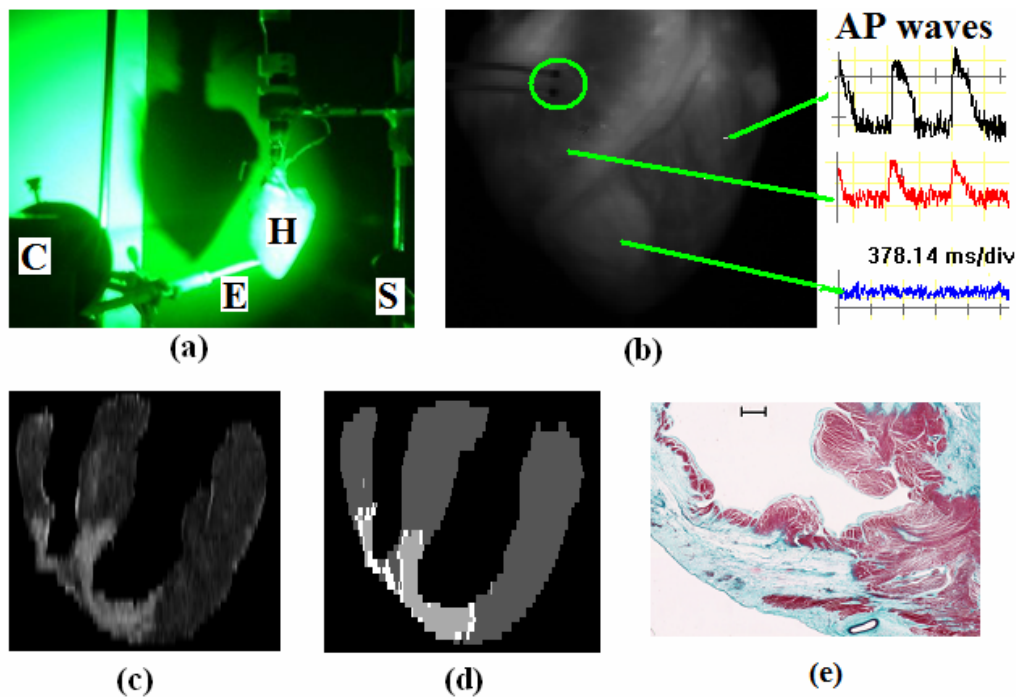


Figure 1 (a) Snapshot of the optical experimental set-up: a high-speed camera (C) records the changes in fluorescence signal after the dye in the heart is excited by a green light source (S); these changes give the AP waves generated by stimulating the heart (H) via an electrode (E); (b) 2D optical image of a pathologic heart (with chronic infarct) and AP waves at different pixel locations (with the tip of stimulator encircled), no AP waves were observed in the dense scar; (c) example of MR image in long-axis view of the heart; the bright signal corresponds to the infarct scar; (d) segmented MR image (gray corresponds to healthy myocardium, light gray to infarct scar, and white to peri-infarct zone); and (e) histopathology of a sample taken from an area between right ventricle and septum, with red stain being up-taken by the healthy tissue and blue stain showing the fibrosis/collagen deposition in the chronic infarct (the bar is 2mm).

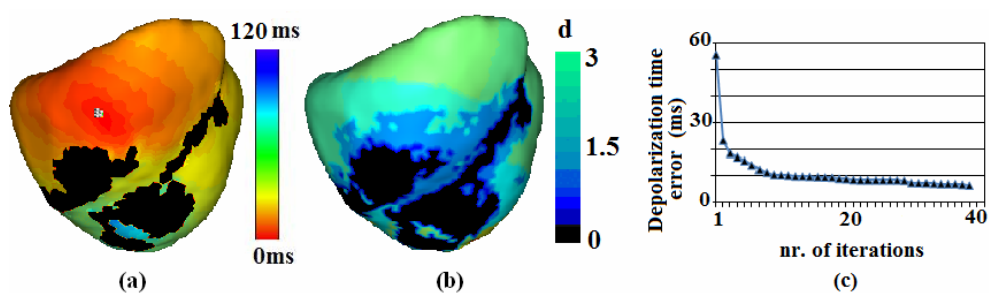


Figure 2 Simulation results obtained in the infarcted heart model (the white dots correspond to stimulation point): (a) predicted isochronal map with early activation times in red (where the stimulus is applied), late activation times in blue and the unexcitable scar (no activation) in black; (b) map of the conductivity parameter “d” after adjustment from measured isochrones (shown is a relative scale for conductivity; with zero value corresponding to the unexcitable scar, and maximum values to healthy myocardium); and (c) error descent of the iterative algorithm.

Sinogram correction methods in MiniPET-II

György Kovács, Sándor Attila Kis, Imre Lajtos, Gábor Opposits, László Balkay, Lajos Trón,
Miklós Emri

Institute of Nuclear Medicine, University of Debrecen, Debrecen, Hungary

The examination of small animals using in-vivo imaging methods is a crucial tool in pharmacy research projects. To suffice this demand, a small animal PET camera (called MiniPET-II) has been built in our Institute of Nuclear Medicine, University of Debrecen, Hungary. We have implemented several image reconstruction algorithms, but due to the high time and computing demand of the 3D iterative and backprojection based reconstruction, in practice 2D methods are used: the data acquired in 3 dimensions is separated into 2 dimensional slices, and then 2D filtered backprojection or iterative reconstruction methods can be applied. Because of our detector system is polygon shaped, we have faced the problem of missing data in the sinograms: there is a small gap between the neighbouring crystals of the neighbouring detectors and there are no coincidence lines going through this gap. Another problem of polygon shaped detectors is the non-uniform distribution of coincidence lines. We have started to work out sinograms adaptive to the scanner geometry to reduce the distortion of non-uniform coincidence line distribution. and during this we have found a new way to solve the missing data problem using fuzzy means clustering.

Our method has been compared to two conventional algorithms on simulated data. For rebinning SSRB method and for reconstruction filtered backprojection was used. The comparison was carried out computing squared distance between the digital phantom and the reconstructed image.

We can state that our method has similar results as the conventional methods, but our method works in coincidence line space instead of sinogram space and does not need the estimation of parameters, thus it is a more efficient algorithm in the sense of noise sensitivity.

Accelerated three dimensional Monte Carlo image reconstruction technique in small animal SPECT

Ziad EL BITAR, Virgile BEKAERT and David BRASSE

*Institut Pluridisciplinaire Hubert Curien UMR/CNRS 7178, Strasbourg, France.
23 rue du loess, 67037 Strasbourg France
e-mail contact : ziad.elbitar@ires.in2p3.fr*

It has already been proved that Fully 3D Monte Carlo (F3DMC) is a robust image reconstruction algorithm that can be applied in Single Photon Emission Computed Tomography (SPECT) and small animal Positron Emission Tomography (PET). The advantage of such image reconstruction technique is that all the physical processes occurring within the detector and its geometrical parameters can be precisely modelled within the system matrix thanks to powerful Monte Carlo simulation toolkit.

In our institute, the ImaBio group has developed and built a small animal multimodality imaging platform called AMISSA that includes a microCT (Computed Tomography) and a microSPECT. The integration of a microPET into the platform is in progress.

F3DMC was used in order to integrate the model of the microSPECT circular detector into the system matrix. Each element (i, j) of the system matrix represents the probability that a photon emitted from voxel i is detected in pixel j. Once the system matrix is computed, it is integrated within the MLEM iterative image reconstruction technique. Geant4 Monte Carlo simulation toolkit was used to model the transport of gamma rays from detector's field of view to the detector.

In order to address for the major drawback of the F3DMC method which is its huge time consumption, two issues were proposed. The first was a parallelisation of the Geant4 simulations for the computing of the system matrix on a computing grid available on the campus of the laboratory and the second was to apply a Forced Detection (FD) technique within the simulations in order to accelerate the convergence of values within the system matrix. The Forced Detection technique consisted in forcing the direction of the emitted gamma rays towards a 2 mm diameter disk centred at the collimator pinhole. No attenuating medium was simulated. A specific treatment of the detected gammas was considered in order to take into account the forced detection.

The computing grid is composed of 80 bi quad-Core Xeon L5420. 12000 Geant4 simulations were performed in parallel modelling the tracks of 1.53×10^{11} gammas. The independency of Monte Carlo simulations was assured thanks to the usage of pre-computed independent random numbers sequences computed from the Mersenne Twister random number generator.

In order to assess the tomographic performance of the image reconstruction technique, a Derenzo phantom fabricated in our laboratory was used. The Derenzo phantom considered is a 30 mm inner diameter cylinder including six equally sized rods quadrants. The rods within the quadrants have respectively the following diameters 0.8, 1.0, 1.2, 1.4, 1.6 and 1.8 mm. The phantom was filled with 4.5 mCi of ^{99m}Tc . A set of 128 acquisitions was performed over 360 degrees with an acquisition time of 30 seconds per acquisition. Projections are sampled into 8×40 pixels of $2.3 \times 2.3 \text{ mm}^2$ each.

The total time required to simulate all emitted gamma is about 28 hours and 20 minutes. This computation time can be optimized if more computing elements are added to the computing grid. The sparse system matrix used for reconstruction has a size of 1.03 GBytes and represents a full matrix of $128 \times 8 \times 40$ rows and $24 \times 96 \times 96$ columns. A total time of 42 s was required to perform 50 iterations using the MLEM algorithm. The reconstructed image of the Derenzo phantom sampled into $24 \times 96 \times 96$ voxels using the F3DMC shows an achievement of a 1.2 mm spatial resolution (figure 1). The study of image quality in terms of quantification and signal to noise ratio as function of the number of simulated gamma is currently in progress.

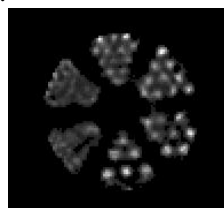


Figure 1. Reconstructed image of the Derenzo phantom.

PART II

Poster Presentations

(In Alphabetical Order)

MC comparison of MA-PMT and SiPM read out schemes for a LYSO block

Pablo Aguiar, Alfredo Iglesias, Cristina Lois and Beatriz Couce
Grupo de Investigación en Radiofísica, Facultad de Física
Universidade de Santiago de Compostela, Galicia, Spain
e-mail: pablo.aguiar@usc.es

Introduction

The development of new detector technologies aims at lowering the limit of achievable spatial resolution, keeping high sensitivity, for PET and SPECT techniques in preclinical small animal imaging. Multi-anode photomultiplier tubes (MA-PMT) are currently the photon detector of choice (giving high gain and fast response) for high spatial resolution readout of scintillator crystal based detector modules. Nevertheless, their relatively low photodetection efficiency (PDE), relatively large size and fragility, and their incompatibilities with MRI high magnetic fields are still a significant drawback. New generation solid state photo-detector devices, Geiger-Müller avalanche photo-diodes or silicon photomultipliers (SiPM), could become the new photon detector of choice mainly due to their high PDE, small size, ruggedness and insensitivity to MRI high magnetic fields.

Methods

We performed Monte Carlo simulations (using Geant4 Application for Emission Tomography, GATE), to evaluate the expected performance of different readout solutions for a monolithic LSO block (50x50mm²), considering several 2D SiPM array configurations (with 8x8 elements) and of conventional MA-PMT (Hamamatsu H8500). The use of discrete SiPMs (with PDE=0.6) was considered for the implementation of the SiPM arrays. SiPM devices of effective areas of 1mm² or 3mm² were spaced by 6 mm in an 8x8 array to cover an area of 50x50 mm² (crystal block size). Configurations with and without reflective material (reflexion index of 0.9) filling the gaps between SiPMs (surrounding diode active area) were considered. MA-PMT (with PDE=0.25) 8x8 pixel (6 mm pitch) readout was simulated for comparison. The same crystal surface treatments were used for different readout schemes: rough entrance face, rough black painted edges and fine polished readout face. Light information is collected by defining a 8x8 array of independent 6x6 mm² square pads. Geometrical parameters and photo-conversion factors describing the different readout configurations are used to estimate photoelectron distributions. Spatial coordinates of gamma-ray interactions were calculated from 2D readout patterns of scintillation light spread functions (LSF) by using Anger logic. A collimated point-source of 149 keV gamma emissions was defined, considering only perpendicular incidence in the crystal entrance face. Main performance parameters like spatial resolution and energy resolution were evaluated.

Results

The average number of collected photoelectrons was 327 phe for MA-PMT read out; 190 phe for the 8x8 3mm² SiPM read out and 46 phe for the 1mm² 8x8 SiPM array readout without reflector in dead zones. When reflector material was included, the number of collected photoelectrons increased to 881 phe for the 3mm² SiPM and 172 phe for the 1mm² SiPM array. As may be observed by comparison (table 1), the read out configuration based on 3mm² SiPM with reflector in dead zones (because of the higher number of photoelectrons), provides higher energy resolution and also better spatial than the MA-PMT solution.

Read out configuration	ΔX (mm)	ΔE (%)
MA-PMT	1,31	28
8x8 SiPM (Area = 1mm ²)	1,93	32
8x8 SiPM (Area = 3mm ²)	0,73	20

Table 1: Spatial and energy resolution for MA-PMT and SiPM array readout of a monolithic LSO block.

Conclusions

Our results show that a detector module based on an array of 8x8 discrete SiPM (3mm²) may lead to significant improvements of spatial and energy resolution with respect to the conventional MA-PMT readout of detector modules based on monolithic blocks. Our findings show that these improvements can be obtained thanks to the idea of introducing a reflector around the discrete SiPMs active area.

Individual CT Phantom for Liver

Farshid Babapour Mofrad^{1, 2}, Reza Aghaeizadeh Zoroofi³, Ali Abbaspour Tehrani-Fard^{1, 4}, Shahram Akhlaghpour⁵, Yen-Wei Chen², Yoshinobu Sato⁶

¹Faculty of Engineering, Science and Research Branch, Islamic Azad University, Tehran, Iran

²College of Information and Science, Ristumeikan University, Shiga, Japan

³Control and Intelligent Processing Center of Excellence, School of Electrical and Computer Engineering, College of Engineering, University of Tehran, Tehran, Iran

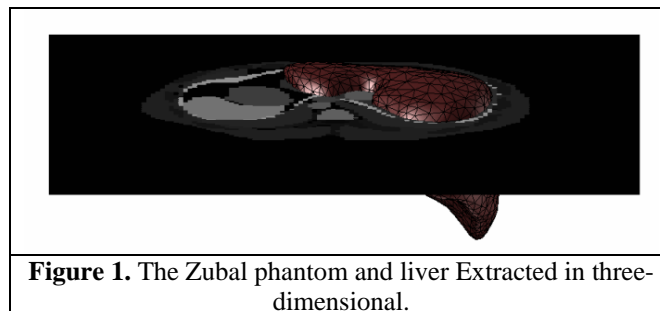
⁴Electrical and Electronic Engineering School, Sharif University of Technology, Tehran, Iran

⁵Departments of Interventional Radiology, Sina Hospital, Tehran University of Medical Sciences, Tehran, Iran

⁶Division of Image Analysis, Graduate School of Medicine, Osaka University, Osaka, Japan

E-mail: Farshid.mofrad@yahoo.com

A powerful and well-known numerical technique for solving statistical problems in nuclear medicine is Monte Carlo (MC) method. The mathematical human phantoms for sampling of radionuclide distortion in two different principles are used (analytical description of a source, and second pixel-based image) [1, 2]. A computational framework is presented for Construction a three-dimensional individual computed tomographic phantom for liver structure using Zubal phantom [3]. The results showed that the propose method is effective for automatic individual phantom construction.



Many robust method for shape modeling, and 3-D processing are used, Spherical Harmonics (SH) Shape description[4] was used for surface modeling, a non-rigid point matching for landmark tagging, the least square method and Thin-Plate Spline [5] for registration. We are now developing a three-dimensional individual phantom for liver from Zubal phantom using combining Spherical Harmonics and Thin-Plate Spline method to improve the accuracy of dosimetry and other nuclear medicine simulation using human phantoms.

References:

- [1] Wernick MN, Aarsvold JN (2004) Emission Tomography. The fundamentals of PET and SPECT, Elsevier.
- [2] Park S, Lee JK, Lee C (2006) Development of a Korean adult male computational phantom for internal dosimetry calculation, 121(3): 257-264.
- [3] Zubal IG, Harrell CR, Smith EO, Rattner Z, Gindi G. Hoffer, PB, (1994) Computerized three-dimensional segmented human anatomy, Medical Physics, 21(2): 299-302.
- [4] Shen L, Farid H, McPeck MA (2009) Modeling 3-dimensional morphological structures using spherical harmonics. Evolution 63: 1003-1016.
- [5] Babapour F, Abbaspour A, Zoroofi R, Akhlaghpour S (2008) Volumetric Non-rigid Registration via Thin-plate Spline Model. APCMBE 2008, 19: 269–272.

Evaluation of Noise Reduction in the SPECT images using wavelet

Babak Ebrahimi, Farshid Babapour, Ali Abbaspour, Dariush Sardari
Faculty of Engineering, Science and Research Branch, Islamic Azad University, Tehran, Iran
E-mail: Farshid.mofrad@yahoo.com

Introduction: SPECT is a diagnostic imaging technique which has the main disadvantage of Poisson noise existence. So far, different methods have been used by scientists to improved SPECT images. Wavelet Transform is a new method for de-noising, which this method is widely used for noise reduction and quality improvement of images. The purpose of this paper is evaluation of noise reduction in SPECT images by wavelet.

Materials and Methods: Simulation using Monte Carlo packages is increasingly used in Nuclear Imaging both for PET and SPECT applications. Either for modeling imaging systems or developing algorithms for analysis and improvement of image quantification. As, in this work, SIMIND software was used to simulate SPECT images. Then, the simulated images (the Jaszak phantom) in the Elliptical collimator with parallel holes types of LEGP (Low Energy General Purpose) are de-noised by types of wavelets and low pass filters in the MATLAB7.5 software.

Discussion and Results: At last, in the Elliptical collimator, the best type of wavelet (bior4.4, 2 wavelet) and the best type of low pass filter ((5*5) low pass filter) is selected (See Fig.1), which they were obtained by testing 114 types of wavelets and 3 types of low pass filters. The results demonstrated that bior4.4, 2 wavelet has increased SNR (Signal to Noise Ratio) 17% more than (5*5) low pass filter and also, bior4.4, 2 wavelet maintained CR (Contrast of Recovery) 29% more than (5*5) low pass filter, furthermore bior4.4, 2 wavelet has decreased CV (Coefficient of Variation) 31% more than (5*5) low pass filter.

Conclusion: Wavelet improved quality SPECT images. Therefore, wavelet is applicable for nuclear medicine image de-noising.

Keywords: SPECT, SIMIND, Simulation, Wavelet, De-noising.

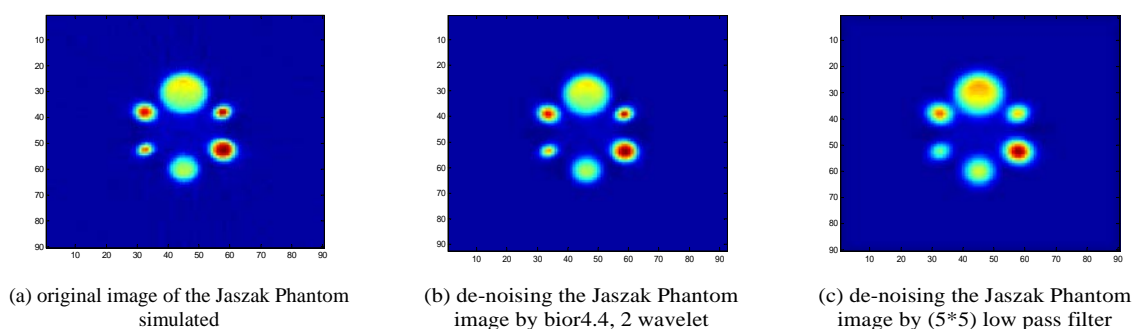


Fig.1. Comparison between original image and de-noising images.

References:

- [1] Y.Y. Shih, J.C. Chen, R.S. Liu, Development of wavelet de-noising technique for PET images. *Computerized Medical Imaging and Graphics*, 29 (2005) 297–304.
- [2] <http://www.radfys.lu.se/simind>.

Simulation of High-Resolution Magnetic Resonance Images on the IBM BlueGene/L Supercomputer using SIMRI

Karl G. Baum, PhD¹ (Karl.Baum@rit.edu), Gary Menezes^{1,2}, María Helguera, PhD¹

¹Biomedical and Multimodal Medical Imaging Lab, Chester F. Carlson Center for Imaging Science, Rochester Institute of Technology, Rochester, New York USA

²Webster Schroeder High School, Honeoye Falls, New York USA

Introduction: Creating software models of the human anatomy and imaging systems, and modeling the medical physics of the imaging acquisition process can provide a means to generate realistic synthetic data sets. In many cases synthetic data sets can be used, reducing the time and cost of collecting real images, and making data sets available to institutions without clinical imaging systems.

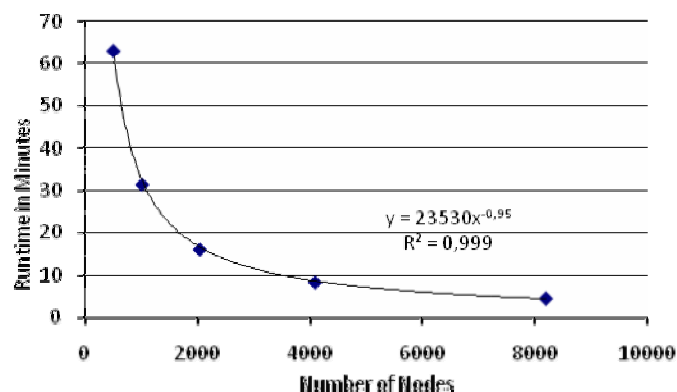
While medical image simulation software has been under development since the 1980s, until recently the complexity of the procedures and long computation times have limited the realism and accuracy of artificially generated images. This is especially true for Bloch equation-based magnetic resonance image (MRI) simulators, in which the evolution of the magnetization of a large number of individual isochromats are modeled.

Methods: SIMRI is a Bloch equation-based magnetic resonance image (MRI) simulator, developed at CREATIS, Lyons, France, designed for small clusters supporting MPI. Modifications were implemented to support the specialized operating system and hardware requirements available on the Blue Gene/L Systems. In particular, this involved optimizing memory usage for both the MPI communication and SIMRI to be sufficiently below the 1024MB limitation of a computational node (virtual memory is not supported by the OS). Additional modifications were necessary to allow increased parallelization within SIMRI in order support and efficiently utilize the large number of compute nodes available on the Blue Gene.

The code was evaluated using two Blue Gene/L systems available in New York. New York Blue is hosted at Brookhaven National Laboratory and consists of 18,432 dual 700Mhz PowerPC 440 nodes with 1024MB of memory. Rensselaer's Computational Center for Nanotechnology hosts another system consisting of 16,384 dual 700Mhz PowerPC 440 nodes divided equally between 512MB and 1024MB configurations.

Results and Conclusions: The code was successfully modified to allow execution on the Blue Gene/L systems. This resulted in, to the author's knowledge, the first system capable of generating high resolution (256^3 voxels) realistic MRI images within a short period of time by directly modeling the Bloch equations. 256^3 voxel simulations can be completed using 8192 nodes in approximately four hours.

The figure below is a plot of run time versus the number of nodes used when performing a 128^3 voxel spin-echo simulation. This plot demonstrates the scalability of the modified SIMRI. As expected run time is inversely proportional to the number of nodes used. The efficiency (speed-up divided by number of nodes) is approximately unity tapering off only slightly as the number of nodes approaches the number of isochromats.



The use of distributed systems such as the Blue Gene/L systems available at Brookhaven National Labs and the Rensselaer Polytechnic Institute provide unparalleled computational capabilities allowing full resolution data sets to be generated in reasonable amounts of time.

Acknowledgements: This research utilized resources at the New York Center for Computational Sciences at Stony Brook University/Brookhaven National Laboratory which is supported by the U.S. Department of Energy under Contract No. DE-AC02-98CH10886 and by the State of New York. This research also utilized resources at the Computational Center for Nanotechnology Innovations at Rensselaer Polytechnic Institute which is supported by New York State and IBM. In addition, this research was supported by Research Computing at the Rochester Institute of Technology.

Benoit-Cattin, H., Collewet, G., Belaroussi, B., Saint-Jalmes, H., and Odet, C., "The SIMRI Project: A Versatile and Interactive MRI Simulator," *Journal of Magnetic Resonance Imaging*, 173, 97-115, 2005.

Design Studies for High Sensitivity DOI Detector for Small Animal PET

Yong Hyun Chung^{1,2*}, Seung-Jae Lee^{1,2}, Cheol-Ha Baek^{1,2}, Ji Yeon Hwang^{1,2}

¹Department of Radiological Science, College of Health Science, Yonsei University, Wonju, 220-710, South Korea

²Institute of Health Science, Yonsei University, Wonju, 220-710, South Korea

In recent years, small animal PET scanners with depth of interaction (DOI) capability have been developed for molecular imaging research. The aim of this study is to perform simulations to design the high sensitivity DOI detector. For this purpose, a small animal PET scanner, employing a dual layer crystals and a pulse shape discrimination scheme, was designed. The proposed scanner has an inner diameter of 88.0 mm with 6 detector modules. Each module is composed of a 5.0 mm thick trapezoidal monolithic-LSO crystal with a front face (surface facing the inside the scanner) of $44.0 \times 44.0 \text{ mm}^2$ and a back face of $50.0 \times 50.0 \text{ mm}^2$ and 23×23 array of LuYAP crystals with a $2 \times 2 \text{ mm}^2$ sensitive area and 15.0 mm thickness. The LuYAP crystals are attached to the Hamamatsu H8500 PMT which has a dimension of $52 \times 52 \text{ mm}^2$ with an effective area of $49 \times 49 \text{ mm}^2$. The ability of the event positioning in the trapezoidal monolithic-crystal was evaluated by modeling the light distribution in the detector using DETECT2000 and the optical treatment of crystal surface was optimized. The sensitivity of the designed PET detector was simulated using the Monte Carlo code GATE. Gamma events were well separated within 2.0 mm spatial resolution in both front and back layers and the new detector shows higher and uniform sensitivity compared to the rectangular detectors since the trapezoidal crystals minimize the dead space within a detector ring. In conclusion, our new detector proved to be a reliable design for small animal PET with high sensitivity by high filling fraction and high spatial resolution by DOI information.

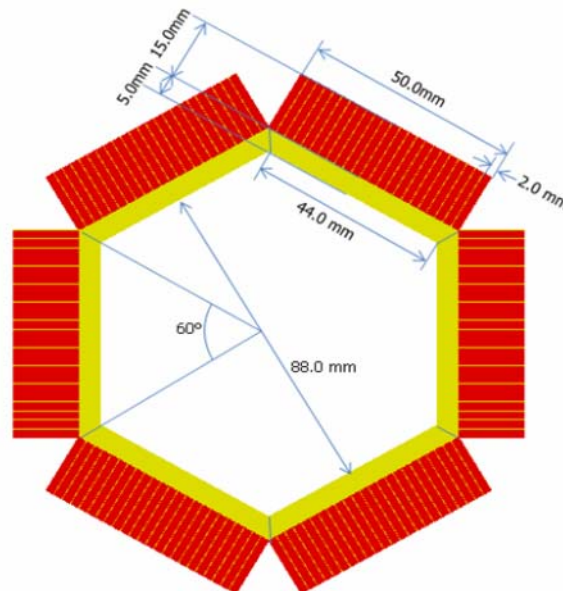


Figure 1. Schematic diagram of a small animal PET. The dual-layer detector module consists of a trapezoidal monolithic-LSO crystal as a front layer and an array of LuYAP crystals as a back layer.

A High Resolution SPECT Detector with Depth-Encoding for Multi-Energy Imaging

Yong Hyun Chung^{1,2*}, Cheol-Ha Baek^{1,2}, Seung-Jae Lee^{1,2}, Ji Yeon Hwang^{1,2}

¹*Department of Radiological Science, College of Health Science, Yonsei University, Wonju, 220-710, South Korea*

²*Institute of Health Science, Yonsei University, Wonju, 220-710, South Korea*

Iodine-125 is one of the widely used radionuclides in the field of experimental oncology and several SPECT systems for I-125 imaging in small animals have been reported. Since I-125 emits low energy photon (27-35 keV), thin crystal about 1.0 mm and collimator are employed to obtain high quality image, however, this scintillator is not useful for Tc-99m imaging because of its low stopping power. Thick crystal used for Tc-99m imaging suffers from poorer intrinsic resolution for I-125 imaging. In this study, depth of interaction (DOI) detection method was applied to 3.0 mm thick CsI(Tl) crystal to acquire high quality SPECT images for I-125 and Tc-99m.

We designed a SPECT detector with DOI measurement capability based on the two-layer monolithic CsI(Tl) crystals coupled to a position sensitive PMT. The proposed detector consists of $50.0 \times 50.0 \times 1.0 \text{ mm}^3$ CsI(Tl) as a front layer and $50.0 \times 50.0 \times 2.0 \text{ mm}^3$ CsI(Tl) as a back layer. For Tc-99m imaging, two layers are considered to be a single crystal and simple Anger logic is used for position estimation. Positions of gamma events in the front layer are determined by a maximum-likelihood position-estimation (MLPE) algorithm with a Gaussian noise model for I-125 imaging. The MLPE algorithm estimates the event position with the measured detector response function (DRF). The main idea of this design is that flint glass layer is introduced during the machine training procedure to make look up tables (LUTs). By replacing the back layer with flint glass which has the same refractive index as CsI(Tl), we can generate gamma events only in the front layer without disrupting the light distribution and can acquire the LUT values experimentally.

Monte Carlo simulation codes, DETECT2000 and GATE were used to evaluate the ability in extracting the DOI information, and to establish the methodology for event positioning in the new detector module. Light transport and detection were modeled in the two-layer detector using DETECT2000, with LUTs built by simulation. To measure the resolution in the front layer, the I-125 gamma events were generated at 49 different points over one fourth of the detector area and the FWHMs were measured. Phantom images were acquired using GATE for I-125 and Tc-99m and the results indicate that high resolution and sensitivity imaging is feasible using the proposed depth-encoding SPECT.

Software for achieving physical analysis on digital systems for medical imaging

B. Donini^a, S. Rivetti^{a,b}, M. Bertolini^c, N. Lanconelli^a D. Acchiappati^b
^a Alma Mater Studiorum - University of Bologna, Bologna - Italy
^b Servizio Fisica Sanitaria "Azienda USL di Modena" Modena - Italy
^c Arcispedale Santa Maria Nuova, Reggio Emilia - Italy

Abstract

The increasing sophistication and resolution of modern medical imaging device leads to an increasing of difficulties in management of the assessment and quality assurance of the quick systems turnover. The large number of technological and physical approach for each imaging modalities proposed by each vendor are so different from one another that each new purchase requires a significant resources deployment to optimize the performances. Researchers and equipment vendors need to work collaboratively to develop the quantitative protocols for imaging, scanner calibrations, and robust analytical software that will lead to the routine inclusion of quantitative parameters in the diagnosis and therapeutic assessment of human health.

The aim of this work is to present a software developed by our group for assisting users in achieving a physical characterization of an X-ray digital imaging system. The software has been implemented as a plugin of the well-known image processing software ImageJ. In this way, all the functionalities of the ImageJ suite can be used with our software. Further, users are facilitated, since the plugin is integrated in a suite widespread and familiar for most of the physicists of the medical imaging community. We believe that this software could be useful to a variety of users: physicists working in hospitals, and more in general, to the staff working in radiological departments, such as medical physicists, physicians, engineers.

The software developed by us can be used with images coming from different modalities (radiology, mammography) and assists users in calculating various physical parameters such as the response curve, Modulation Transfer Function (MTF), Noise Power Spectra (NPS), Detective Quantum Efficiency (DQE). In particular, the MTF can be estimated both with the slit and the edge techniques. Results can be displayed as text and graphical plots and can be exported for further processing. All the operations can be done in a very easy and friendly way, thanks to the strict interconnection with the ImageJ framework.

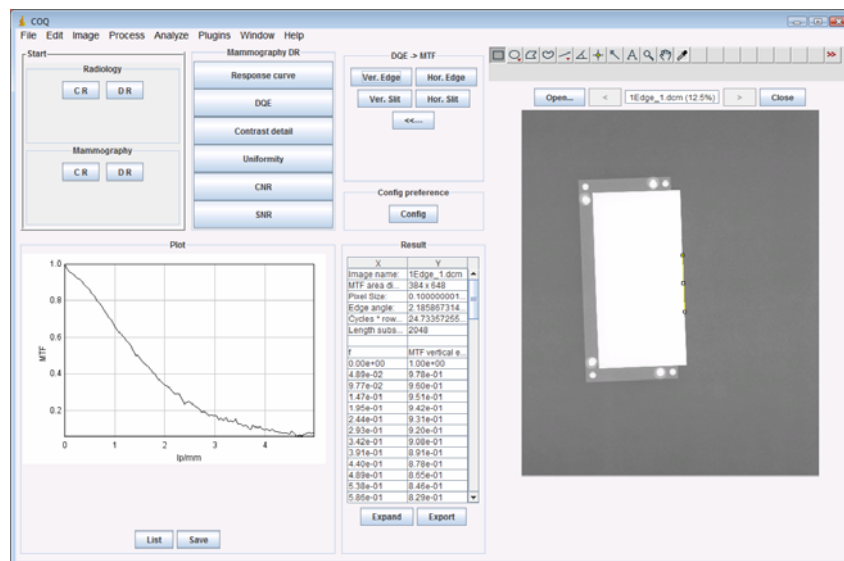


Figure 1: Main window of the ImageJ plugin developed for performing the physical analysis.

Microtomography: an accurate and low-cost method to assess body composition and bone parameters in a same animal over time

Habold Caroline and Brasse David

Institut Pluridisciplinaire Hubert Curien; UMR 7178 CNRS/IN2P3-ULP, 23 rue du Loess, BP28,
67037 Strasbourg Cedex 2, France

caroline.habold@c-strasbourg.fr, david.brasse@ires.in2p3.fr.

There are increasing demands from physiologists studying energetic metabolism and from ecophysiologists to measure body composition or bone metabolism *in vivo* in a same animal over time. The common techniques to evaluate body composition in animals are dual energy X-ray absorptiometry (DEXA), total-body electrical conductivity (TOBEC), bioimpedance and doubly labelled water, but these techniques do not give spatial information on the distribution of adipose tissue. Computed tomography and magnetic resonance image (MRI) scanning are the only widely available methods that precisely and accurately distinguish between different fat pads. Bone metabolism is also extensively studied through several densitometric methods. The use of computed tomography for bone studies in small animals (microCT) provides advantages over past methods, because it provides a true volumetric bone mineral density (BMD) and can discriminate between cortical and trabecular compartments. Also, microCT increases resolution and is an imaging technique that gives information on bone microstructure

In the present study, we tested whether microCT can provide *in vivo* an accurate measure of visceral and subcutaneous adiposity, muscle volume and bone volume, mineral content (BMC) and BMD. In that way, mice (n=10) were scanned at an isotropic voxel size of 100 μ m (40 kVp, 250 μ A, 500 ms integration time) with the microCT system developed by our institute. Mice were then killed by cervical dislocations. Upon euthanasia, two distinct fat pads were harvested and weighed: the visceral fat pad and a subcutaneous fat pad spanning the abdominal and gluteal regions (between the lower part of the rib cage and the tail). Also, the tibiae as well as the hindlimb muscles were harvested and weighed. Furthermore, all the samples were scanned *ex vivo* by microCT according to the same conditions as *in vivo*. The volume of the visceral and subcutaneous fat pads, of the hindlimb muscles and of the tibiae as well as the BMC and the BMD of the tibiae were evaluated on the microCT projections. Fat volume values were converted to fat weight by using the average density of triglyceride (0.900 kg/L).

The *in vivo* microCT scans provided a sufficiently high contrast and signal-to-noise ratio to identify and isolate adipose tissue, muscles and bones throughout the body of the mouse. The use of skeletal sites as anatomical landmarks allowed the precise definition of the regions of interest. The weight of the visceral and of the subcutaneous adipose tissues obtained *in vivo* on microCT scans were closely correlated with the physiologic weight of these tissues removed at sacrifice, and were positively correlated to body mass. Also, there were significant positive correlations among the volume values of the hindlimb muscles obtained *in vivo* and those obtained *ex vivo* after dissection. Finally, the BMC and bone volume of tibiae determined *in vivo* on microCT scans of living mice were closely correlated with the mineral content and volume of these bones removed at sacrifice and scanned. However, the BMD of the tibiae determined *in vivo* had no explanatory power with respect to the value obtained *ex vivo* because of beam hardening effects that differ whether studies are done *in* or *ex vivo*. These effects will be corrected in a future work through microCT algorithm modification.

MicroCT would be a valuable tool for studies involving measurements of body composition and bone structure in a same animal over time. The advantages of microCT analysis include highly quantitative measurements, small coefficient of variation and the capability for serial measurements in the same living animal.

Evaluation of a commercial multi-channel readout system for PET/SPECT

Alfredo Iglesias, Cristina Lois, Pablo Aguiar, and Beatriz Couce
Grupo de Investigación en Radiofísica, Facultad de Física,
Universidade de Santiago de Compostela, Galicia, Spain
e-mail: alfredo.iglesias@usc.es

Introduction

Recent developments of high performance gamma detection modules (for small gamma camera, PET or SPECT systems) are based on multi-anode PMT devices. Individual anode readout allows optimize detector performance, mainly by channel gain compensation and light spread function (LSF) advanced positioning algorithms, and therefore a large number of channels readout is needed. We report on the evaluation of a new dedicated compact and low cost electronics interface (with user-friendly system-controlling software) for charge integration, acquisition, processing and storage of 64 separate data channels from a multi-anode PMT assembly employed for the development of our detection system prototype.

Material and methods

A new gamma camera module based on a continuous LYSO (51 mm x 51 mm x 4 mm) scintillator slab coupled to a multi-anode device Hamamatsu H8500D is been developed. The MAPMT is operated at high gain ($G = 2.2 \cdot 10^6$, HV = -1000 V), and the 64 channels are individually read by using a commercial multi-channel charge integrator front-end system. The recently available commercial DAQ system Photonique IQSP582 (Vertilon Corporation, www.vertilon.com), developed for multi-channel PMT readout has been chosen. It is a compact (desk-top), modular, 64 channel system (scalable to 256), with individual channel gain compensation, showing large dynamic range (55fC - 500 pC per channel), high rate capability, variable integration time (from 100 ns), allowing different trigger mode configurations and possibility of on-line event filtering.

Results

Main characteristics of the system have been evaluated (including dynamic range, gain uniformity, crosstalk among anodes, data rate capability, etc.) Basic performance of the detection module has been characterized, in terms of energy resolution and linearity, capability of 2D readout of individual event LSF, LSF signal-to-noise ratio and estimation of number of photoelectrons. Event (singles) rate capability of more than 40 kHz has been demonstrated. Energy resolution of 13% was obtained for ^{22}Na 511 keV photon peak. A detailed characterization study of energy spectra and average LSF for several isotopes (^{241}Am , ^{57}Co and ^{22}Na) and different crystal scintillator block surface configurations (black or reflective) allowed the understanding of light transmission, reflection and collection effects and the validation of a GATE (GEANT4 application) MC simulation model of the detector module. 2D readout of individual LSF events (showing good S/N), allows ongoing activities on the evaluation of different advanced positioning algorithms aiming at high intrinsic spatial resolution and large useful field of view (UFOV).

Discussion and conclusions

The use of a new commercial compact multi-channel DAQ system provides an efficient and easy to use solution for individual anode readout needed for the development of high performance gamma detection modules.

Detector Characteristics and Its Operating Characteristics for X-ray Scanner

Kwang Hyun Kim^a, Jae Yong Jun^b, Jun Young Yang^b

^aSchool of Dentistry, Chosun University, Seosuk-Dong, Dong-Gu, Gwangju, South Korea

^bRadTek, Research Center and Co., LTD, Dukjin-Dong, Yusung-Gu, Daejeon, South Korea

The X-ray scanners are used in various inspection fields and their scan speed is critical in terms of application areas. Other factors to be considered are the gain of the scanner and the effect of image lag for scanning mode. However, the speed, the gain, and the image lag are not only dependent on the photodiode but also electronic circuit. In order to fabricate an optimum system for the given requirements, the optimum design should be driven through trade-off between three factors for the applications. In this research, we have designed and fabricated three PIN type photodiodes and two front-end electronic circuits. Using the combination of the photodiodes and the circuits, we have analyzed their electronic characteristics and radiation response. The photodiodes have the same structure but different specific resistivities of 0.1 kΩ·cm, 0.2 kΩ·cm, 1.0 kΩ·cm, and 5.0 kΩ·cm. The circuits are based on switching integrator and charge sensitive preamplifier (C-Amp.), respectively. The block diagrams of the fabricated the tested several X-ray scanner modules are drawn as bellows.

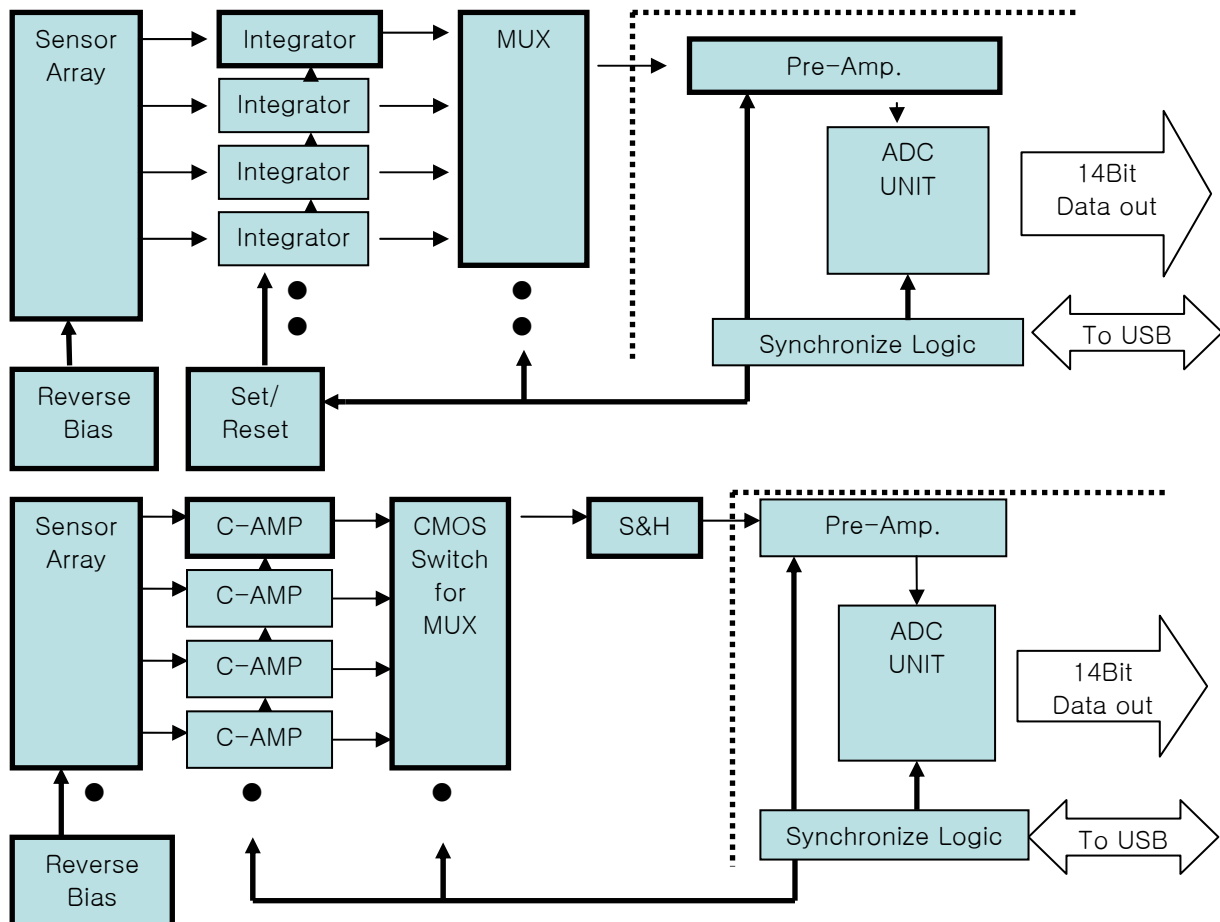


Fig. 1. The Block Diagram of X-ray Scanner using JFET operation amplifier as an Integrator and a charge amplifier.

New Design of Dual Energy X-ray and Its Performance for Several Radiography Conditions

Kwang Hyun Kim^a, Han Kook Shin^a, Jun Young Yang^b

^aSchool of Dentistry, Chosun University, Seosuk-Dong, Dong-Gu, Gwangju, South Korea

^bRadTek, Research Center and Co., LTD, Dukjin-Dong, Yusung-Gu, Daejeon, South Korea

Dual energy X-ray radiography is a useful technique in medical, industrial, and security applications to acquire more detail information. Generally, there are two hardware manipulations; X-ray source and X-ray detector. In the X-ray source manipulation they have used mainly X-ray tube voltages switching and K-edge filtering methods in order to acquire dual energy X-rays. In the X-ray detector manipulation two detectors stacked horizontally are used to acquire dual energy radiographies. In this research, we have suggested new concepts of generating dual energy X-rays and acquiring dual energy radiographies. By using Erbium and Rhodium materials as K-edge filters coincidentally, two parallel low and high-energy X-rays are generated, entering two detectors separately. This new concept may give another option to generate two X-ray energies and better image performance compared to other existing methods. In this research, we have presented the possibility of new idea to apply for dual energy radiography in medical, industrial, and security applications. After selecting representative examples in each application, we have simulated several evaluation parameters, by using Monte Carlo code of MCNPX, such as X-ray beam hardening, entrance exposure, detector signal, separation degree in mixture objects, and contrast image. In each application, we have compared our new idea to other methods. More detail results and analyses will be presented.

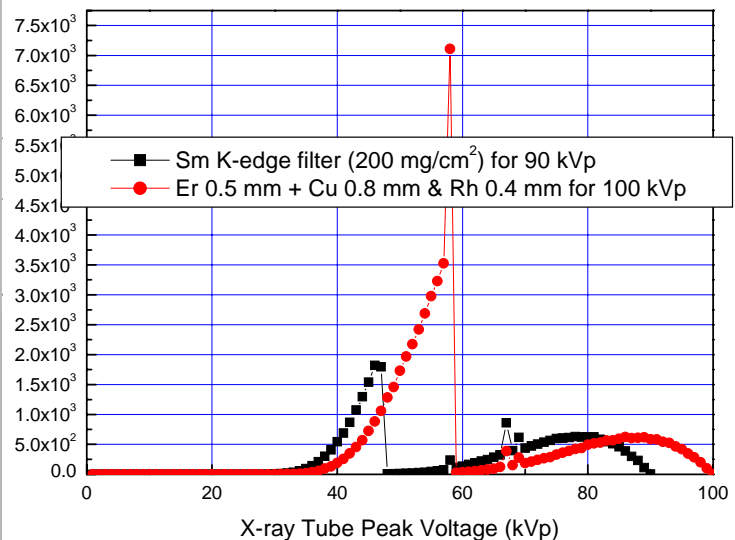
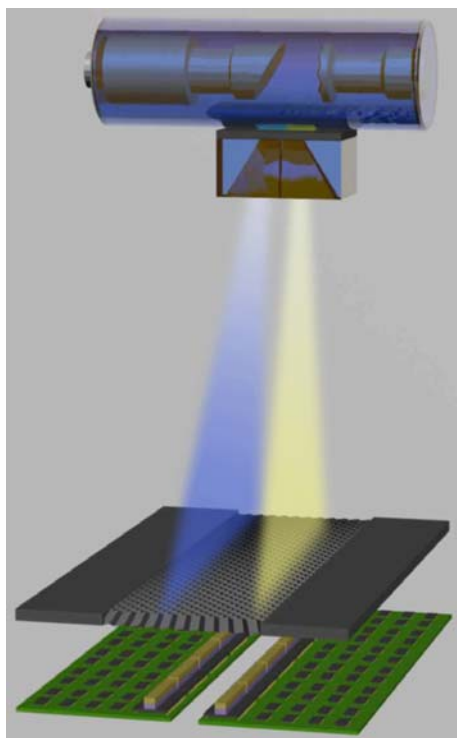


Fig. 2. Simulated examples for new idea and other existing spectrum.

Fig.1. New design of parallel two X-ray beams using single exposure.

Characteristic of X-ray and Gamma-ray Detection for Single Channel Photodiode and Amplifiers

Kwang Hyun Kim

School of Dentistry, Chosun University

Single channel photodiode, charge sensitive preamplifier, and shaping amplifier have been designed and fabricated for the tests of X-ray and gamma-ray detections. The PIN type photodiodes with $1 \text{ k}\Omega \cdot \text{cm}$ of $1 \text{ cm} \times 1 \text{ cm}$ coupled with several scintillators are connected to our own fabricated charge sensitive preamplifier based on ASIC and shaping amplifier integrated on test board. The photodiodes fabricated in ETRI have showed their dark currents of below 10 pA at zero bias and quantum efficiency of 88% at the wavelength of 550 nm . The preamplifier fabricated in high voltage of CMOS $0.7 \mu\text{m}$ is folded cascade type and the shaping amplifier based on operational amplifier has been fabricated on PCB. Each component will be tested for the view of signal and noise. The totally integrated detector modules have been tested under the radiation condition of dual photon and dual energy X-ray absorptiometry. Each test result will be compared with a commercial CZT detector module of eV product and analyzed for both X-ray and gamma-ray. From the results of this work, the limit and possibility of the detector based on scintillator coupled photodiode module for each radiation application will be discussed in detail.

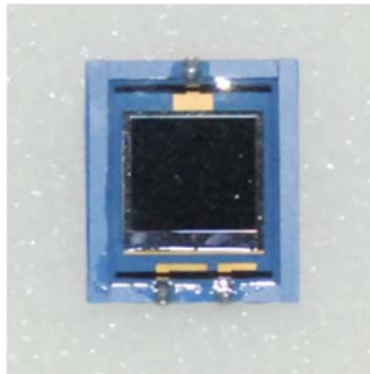


Fig.1. PIN type photodiode of $1 \text{ cm} \times 1 \text{ cm}$.

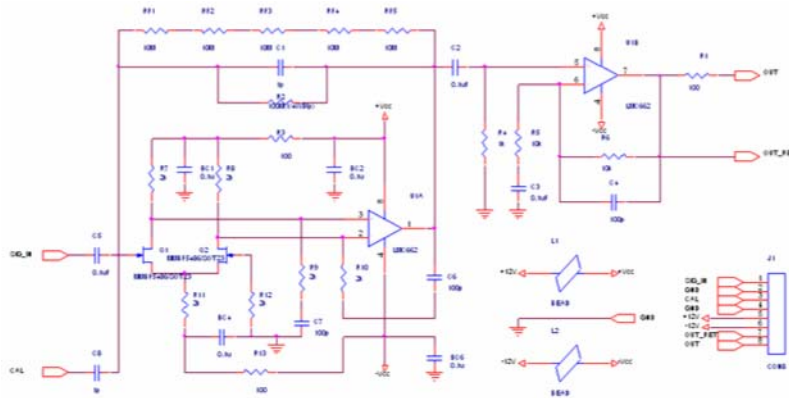


Fig.2. Diagram of folded cascade preamplifier.

RADIOPHARMACEUTICAL (Sm 153 - EDTMP) BONE PALLIATIVE TREATMENT AND MONTE CARLO SIMULATION

N. Lagopati, M. Sotiropoulos, M. Andreou, J. Vamvakas,
G.S. Limouris, M.E. Lyra*

A' Department of Radiology, Section of Nuclear Medicine, University of Athens,
Aretaeion Hospital

Introduction: Radiopharmaceutical Samarium 153 – EDTMP (ethylenediamine tetramethylene phosphonate) palliative treatment remains the method of choice for painful skeletal metastases. The physical characteristics of samarium, with a half life of 46.27 h, beta emissions of 0.64, 0.71 and 0.81 MeV and a 0.103 MeV gamma emission, permit optimum internal radiotherapy with prospective estimation of radiation dose to metastases and bone marrow in each patient, so to maximise dose in the target and minimize the side effects.

Purpose: To compare absorbed doses by scintigraphic planar images data (by Elscint Apex 4 SPX tomographic gamma camera) and Monte Carlo (MC) simulation (Monte Carlo N- Particle Code (Extending version – MCNPX)), which models the same dosimetry problem.

Materials and Methods: Planar data (anterior and posterior images) of 8 patients with skeletal metastases, in a time period of 1 hour up to 2 days post injection were acquired and used for an estimation of the dose in the lesions of interest, according the MIRD schema. Also MCNPX code was utilized in order to justify the accuracy of the internal dosimetry with the MIRD method, by simulating the distribution of the radioisotope in the region (volume) of interest (ROI) and calculating the absorbed doses in the metastatic lesion, as well as in critical organs.

Results: In order to make a comparison between the absorbed dose in the metastatic lesion area and the equivalent in critical organs, the following ratio is used, named Dose Index (X), for both MIRD and MC.

$$X = \frac{D_{\text{lesion.area}}}{D_{\text{critical.organ}}}, \text{ where } D_{\text{lesion.area}} : \text{absorbed dose in the metastatic lesion area}$$

and $D_{\text{critical.organ}}$: absorbed dose in the critical organ
(red marrow, kidneys, bladder)

Conclusion: There was a good agreement between the results, derived from the two pathways, the real and the theoretical, with a deviation less than 9% for planar data comparing to MC. From this point of view, the applied method for creating the voxel model is validated.

An experimental apparatus for analyzing the physical properties of biological tissues

A. Turco^a, D. Bianchini^a, L. Roma^b, P.L. Rossi^a, N. Lanconelli^{ac},
G. Baldazzi^{ac}, A. Margotti^c, M. Bello^d, N.M. Uzunov^{de}

^a Alma Mater Studiorum - University of Bologna, Viale Berti-Pichat 6/2, 40127 Bologna, Italy

^b S.Orsola-Malpighi University Hospital, O.U. of Radiology, via Massarenti 9, 40127 Bologna, Italy

^c INFN Bologna, Viale Berti Pichat 6/2, 40127 Bologna, Italy

^d INFN-LNL Legnaro, Viale dell'Università 2, 35020 Legnaro (PD), Italy

^e Department of Natural Sciences, Shumen University, Shumen, Bulgaria

1. Abstract

The studies of X-ray attenuation of biological tissues are connected to the possibility of visualizing pathological tissues using new X-ray imaging techniques such as Multi-Energy subtraction X-ray Imaging. In fact the ability to distinguish pathological tissues is strictly related to an accurate knowledge of the X-ray absorption coefficients. A study of the attenuation properties of tissues was started at the University of Bologna in a facility based on a Bragg monochromator. The target of the Bragg monochromator is a LiF crystal able to produce monochromatic beams in a range of energies from 10 keV to 60 keV and with an energy resolution less than 2.0 keV. The absorption data are acquired by a CdTe detector. The energy resolution deterioration caused by the tailing effect at high energies is studied by a comparison with an HPGe detector. We implemented different algorithms for extracting chemical-physical information from X-ray absorption measurements, such as effective atomic number and electron density.

The aim of this work is to present an instrumentation dedicated to the measure of the absorption coefficient of materials, in particular biological samples. An important feature of this apparatus is the possibility of selecting the energy of interest with high precision and repeatability. In addition, a study of the energy resolution of CdTe detector is reported, with a comparison with the energy resolution obtained with an HPGe detector for all the analyzed energy ranges. This study also analyzes the error propagation on the absorption curves, and evaluates the error introduced by the intrinsic characteristic of the detector used.

2. Materials and methods

Our facility comprised an X-ray monochromator based on a Bragg crystal of LiF, three collimator stages to define an X-ray spot-area of analysis on the sample and a rotating stage that supports the tissue sample and the spectrometric detector.

2.1. Monochromatic X-ray facility and detection system

The primary polychromatic X-ray beams are produced by a W anode tube and collimated to an LiF crystal mounted on a rotating stage. Adjusting different crystal angles, the diffraction described by the Bragg law permits to produce quasi-monochromatic X-ray beams with selectable energy. Sample and detector positions are defined by using a second rotating stage, connected to the first one, in order to collect only the X-ray beam transmitted by the sample. In front of the sample, a lead collimator stage defines an X-ray spot of 1 mm² and stops all photons scattered with different angles. An XR-100T-CdTe detector (AMPTTEK, Bedford, MA, USA) cooled by Peltier cells, with dedicated compact spectrometric chain, detects the spectra. In order to correct the CdTe spectra for the incomplete charge collection called hole-trapping, a correction software based on Hecht theory is implemented.

2.2. Energy Resolution of CdTe and HPGe detectors

Absorption spectra are usually acquired with an HPGe detector, that is the most accurate kind of spectrometric detector. The main drawback is that it needs a cumbersome cryogenic cooling system and a dedicated spectrometric chain. With the XR-100T-CdTe detector it is possible to acquire spectra without a cryogenic system and with a very compact spectrometric chain, but it becomes necessary to evaluate and correct the distortion on energy resolution, introduced by the intrinsic effects of this kind of detector. For this reason, a comparative study between the energy resolution obtained using the CdTe detector and the energy resolution obtained using an HPGe detector is presented. In this way we are able to estimate the error on energy values introduced in absorption measurements. The energy resolution is in fact the most critical parameter, that introduces the largest spreading in the analysis algorithm. For a correct evaluation of energy resolution distortion, two Am²⁴¹ spectra were acquired with the two spectrometric systems in the same geometric condition.

2.3. $\mu(E)$ determination by spectrometric measures

In our procedure, two energy spectra are acquired: a reference spectrum, obtained with no tissue inside the graduated test-tube, and the sample spectrum, that represents the transmitted photons through the tissue. Obviously, measured attenuation coefficients are greatly dependent on the energy resolution of the facility.

In fact, the μ values will be defined for a single energy only if the energy peak spectra could be represented by δ -Dirac functions: in our set-up, the FWHM remains less than 1.5 keV for all the energy peaks below 40 keV. It is important considering that the energy range from 10 keV to 40 keV seems to be the most interesting to define the differences between tissues: increasing the X-rays energy, the scattering cross sections decreases, thus reducing the probability to find differences between tissues in the $\mu(E;Z)$ curves.

Characterization of Lu background distribution on a LYSO block

Cristina Lois, Alfredo Iglesias, Pablo Aguiar and Beatriz Couce
Grupo de Investigación en Radiofísica, Facultad de Física,
Universidade de Santiago de Compostela, Galicia, Spain
e-mail: cristina.lois@usc.es

Introduction

Considering the use of a LSO/LYSO crystal block for the development of gamma detection modules shows interesting design features (high detection efficiency, high light yield, fast response, etc.). Despite there is a common opinion that LSO/LYSO is a less valuable material for single photon detection, we have considered the use of a LSO/LYSO monolithic crystal block for the development of small gamma cameras, SPECT and PET detection systems. Concerns on the use of LSO/LYSO for single photon detection systems are due to a significant rate of background signals produced by the presence of the naturally occurring isotope ^{176}Lu (2.6% of natural Lu), which decays by a 420 keV (mean) β emission, followed by prompt gamma emission with energies of 307 keV (94%), 202 keV (78%) and 88 keV (15%).

Methods

A monolithic LYSO block (Prelude 420, 51 mm x 51 mm x 4 mm size, with reflective painted entrance face and black painted edges), coupled to a MAPMT (Hamamatsu Photonics H8500D), with 64 channel readout, was used as basic detection module in this study. 2D images of gamma interaction distributions were generated. Points of interaction were determined from light spread function (LSF) centroids using Anger logic and non-linearity correction based on polynomial fit of non-linear effects along the field of view (FOV).

Results

Peaks corresponding to the known emissions of ^{176}Lu are evidenced on the intrinsic full spectrum of the ^{176}Lu decay (with no external sources present) obtained with open window acquisition (with a 10 keV threshold). A total background rate of 2800 cps (on a 10 cm³ block) has been measured, corresponding to an intrinsic rate of 280 cps/cm³. Lu background acquisition using a low energy window (around 60 keV) showed a non-uniform distribution of counts along the FOV, with minimum background rate at the centre of the FOV (CFOV). This motivated a detailed study of Lu background spatial distribution using different energy windows corresponding to different isotopes. Background count rate profiles along the LYSO block were analyzed, and the useful FOV (UFOV) were defined in terms of Lu background count rate (Lu "background-clean" FOV). Total background rates of the order of 100-800 cps have been observed for different energy windows. For a 200 keV wide window centred at 511 keV the count rate was 822 cps (82 cps/cm³, one-third of the total counts in the spectrum). For a 80 keV window centred at 140 keV and for a 30 keV window centred at 60 keV, the count rates were 213 cps (21 cps/cm³, 7% of the total) and 177 cps (18 cps/cm³, 4% of the total) respectively. These results correspond to total background rates considering the full FOV, but reduced rates are corresponding to the CFOV.

Discussion and conclusions

The low energy component of Lu background spectrum is related to partial energy deposition of decays mainly produced near the crystal edge (showing a hot-perimeter artifact), while total energy deposition (resulting in higher energy events) is produced by decay emissions in the central volume of the crystal block. However, on small segmented LSO/LYSO crystals, with typically 15% dead zones due to gaps between a few mm wide crystals, a higher fraction (uniformly distributed) of partial energy deposition events are produced along the full FOV. Results indicate that when using LSO/LYSO monolithic crystal blocks, ^{176}Lu background is not expected to significantly deteriorate the performance of single photon detection systems.

Validation of GATE optical transport simulation of monolithic LYSO crystal blocks

C. Lois, P. Aguiar, A. Iglesias and B. Couce
Grupo de Investigación en Radiofísica, Facultad de Físicas
Universidade de Santiago de Compostela, Galicia, Spain
e-mail: cristina.lois@usc.es

Introduction

Most small animal PET and SPECT systems in use include pixelated scintillation crystals in order to improve spatial resolution. Nevertheless, these detector modules exhibit greater light loss and consequently lower energy resolution, and furthermore they increase the cost and complexity of the system. We consider the use of a continuous LYSO crystal block read out by a MA-PMT (multi-anode photomultiplier) for the development of high performance gamma detection modules. The aim of the current work is the validation of a detailed simulation model performed on GATE Monte Carlo (MC) package accurately describing light production and optical transport in a monolithic LYSO scintillator block.

Methods

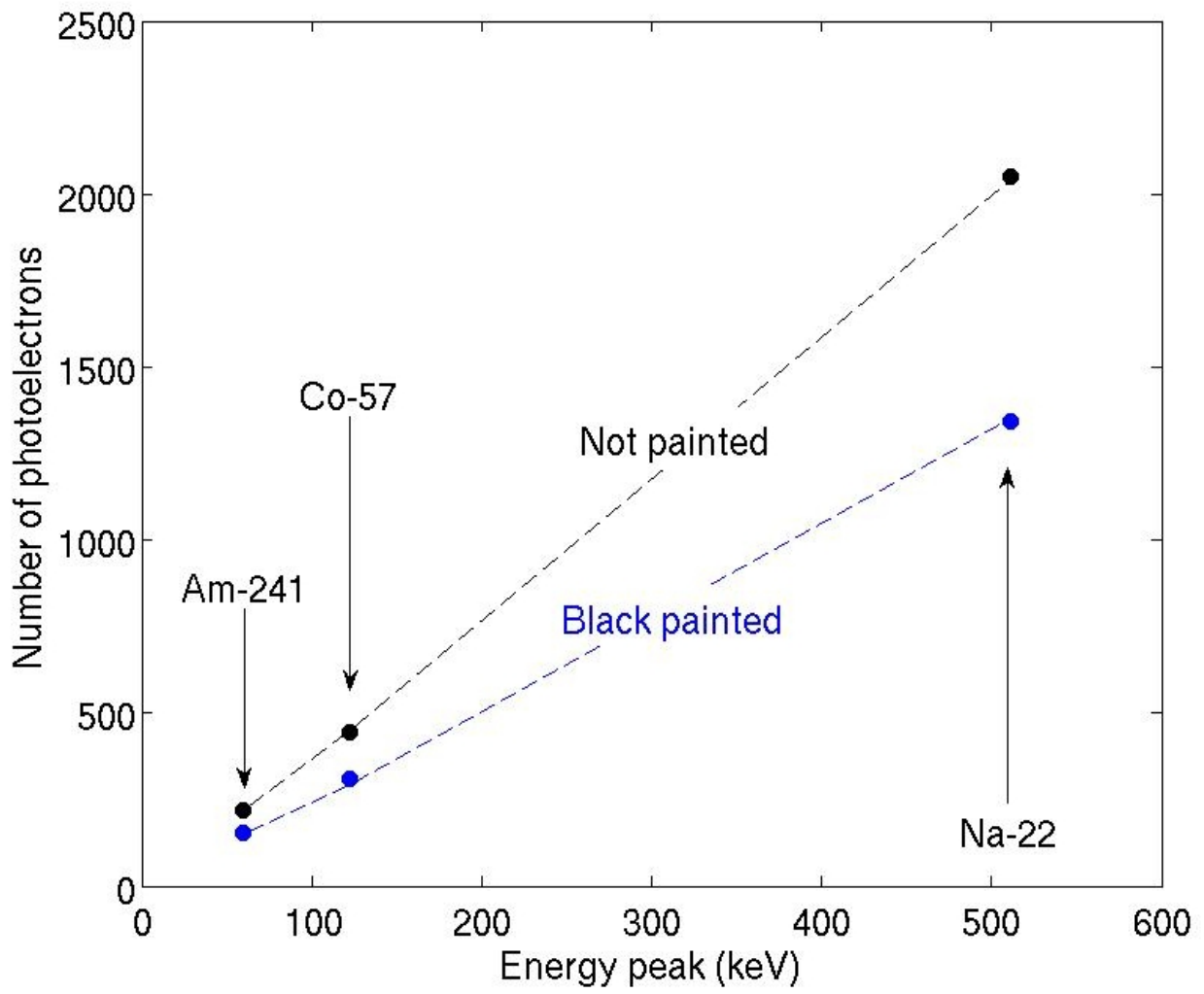
A detection module prototype was developed and basic experimental measurements were performed for MC model validation. The module is based on a 51 mm x 51 mm x 4 mm LYSO (Prelude 420) crystal block optically coupled to 64 pixel MA-PMT (Hamamatsu H8500D). A new commercial multi-channel DAQ system (Photonique IQSP582, from Vertilon Corporation) was used for individual channel readout. The surface of the crystal in contact with the MA-PMT window was fine polished and the side surfaces were ground and black painted. In order to carry out this MC model validation under different light transport conditions, two different surface finish of the entrance (gamma incidence) face were considered: a rough black painted surface (low reflection), and a rough not painted surface in contact with air (medium-high reflection). Point-sources of gamma emitters of various energies: 59.5 keV (241-Am), 122 keV (57-Co) and 511 keV (22-Na) were used considering only perpendicular incidence in the crystal entrance face. Spatial coordinates of gamma-ray interactions in the crystal were calculated from scintillation light spread functions (LSF) by using simple Anger logic. Monte Carlo (MC) simulations were carried out using the Geant4 Application for Emission Tomography (GATE) because it allows us to simulate the optical light production and transport and to include crystal surface treatments, which are essential for an accurate validation of the detector model. Different parameter values were adjusted related to light yield, crystal surface treatments, optical coupling or window thickness and photo-detection efficiency.

Results

A first validation approach of the simulation model was performed in terms of the average number of photoelectrons measured from light production corresponding to the emission peaks of the different gamma-emitters. In addition, further validations have been performed, in terms of energy resolution, related to deviations on the number of photoelectrons; and mean detector response function (MDRF), related to spatial distribution of photoelectrons. A good agreement was found on the experimental and simulated MDRF (at CFOV) comparison. Only energy resolution comparison showed a slight underestimation from the MC simulations with respect to the measured data. Figure 1 shows a comparison between the measured (lines) and simulated (points) number of photoelectrons for both surfaces finish configurations. An excellent agreement between experimental and simulated data was obtained.

Discussion and conclusions

A validation of a simulation model implemented in GATE Monte Carlo (MC) package accurately describing light production and optical transport in a monolithic LYSO scintillator block has been performed. Comparison of measured and simulated average number of photoelectrons, MDRF and energy resolution obtained for various gamma-emitters shows a very good agreement. This validated MC simulation model of a basic monolithic LYSO crystal block is a very useful tool which will allow evaluation of performance for different module configurations, and optimize crystal treatments, optical coupling or crystal thickness for a specific application.



Optical Transport Study for γ -Camera Imaging Devices

M. Mikeli, L. Ragousis, D. Thanasas and E. Stiliaris*

Physics Department, National & Kapodistrian University of Athens, GR-15771 Athens, Greece

Abstract

The light distribution derived from continuous and pixelated crystals used in γ -Camera imaging devices depends on the geometrical and optical characteristics of the scintillation crystal for a given energy of the radiation source. In this work, the optical photon distribution has been studied through Monte Carlo simulations using the transport program DETECT2000. In parallel, systematic measurements for a group of inorganic homogeneous crystals of CsI(Tl) with 2mm, 4mm, 8mm, 12mm and 20mm in thickness, of BGO with 2mm, 3mm, 5mm and 8mm, as well as of a CsI(Tl) pixelated one of 4mm in thickness, have been performed for ^{60}Co , ^{137}Cs and $^{99\text{m}}\text{Tc}$ radiation sources. These data were obtained from a Position Sensitive PhotoMultiplier Tube (R2486 HAMAMATSU) with a 16X+16Y multi-wired crossed anode. Comparison between experimental and simulated results indicates that the collected light is strongly correlated to both the Depth of Interaction (DOI) and the geometrical properties of the crystal. The experimentally obtained parameters for the produced light distribution are expressed and categorised according to the crystal's geometrical characteristics.

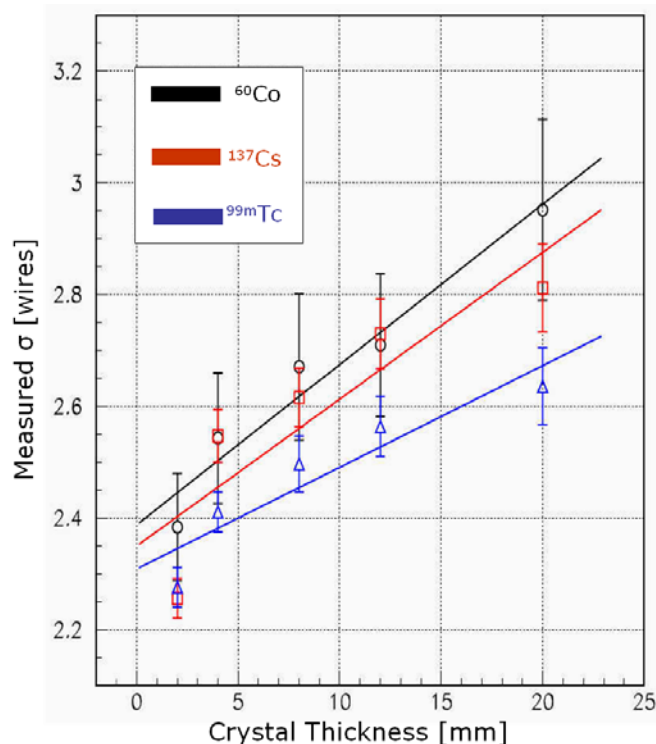


Fig.1 Measured light distribution width (σ) in various CsI(Tl) homogeneous crystals for three different γ -radiation sources. The unit in σ is defined in wire distance ($\sim 6\text{mm}$).

(*) The financial support by the program KAPODISTRIAS (Special Account for Research Grants) of the National and Kapodistrian University of Athens is gratefully acknowledged.

Corresponding author: E. Stiliaris (email: stiliaris@phys.uoa.gr)

Comparison of Breast Tumor Imaging with ^{99m}Tc Radiolabeled PR81 and its F(ab')_2 Fragment

M. Salouti^{*1}, M. H. Babaei², H. Rajabi³, H. Forootan², M.J. Rasaei⁴, A. Bitarafan⁵, M. Shafiee², M. Mazidi², F. Johari Daha²

^{*1}Department of Biology, School of Sciences, Islamic Azad University- Zanjan Branch

²Department of Nuclear Research Center, Atomic Energy Organization of Iran

³Department of Medical Physics, School of Medical Sciences, Tarbiat Modarres University

⁴Department of Medical Biotechnology, School of Medical Sciences, Tarbiat Modarres University

⁵Department of Nuclear Medicine, Shahid Rajaei Hospital

Objectives

Compared to intact IgG, F(ab')_2 and Fab exhibit significantly improved tumor specificity and intra tumor penetration in animal models. Generally, lower molecular-weight agents provide better target to non target ratios due to their rapid background clearance. In this study we compared the biodistribution and localization characteristics of ^{99m}Tc labeled intact PR81 and its F(ab')_2 to identify potentially more useful radiopharmaceutical for diagnosis of breast cancer.

Methods

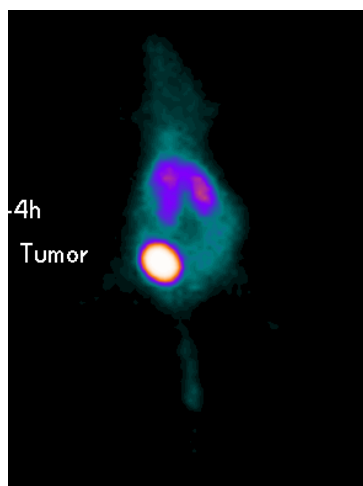
Purified monoclonal antibody PR81 was digested with 5% (w/w) pepsin for 28 hours at 37°C in 0.1 M sodium acetate buffer Ph 4.2. The F(ab')_2 fragments were purified by protein A column chromatography followed by elution with pH 8. The purity of F(ab')_2 preparation was evaluated by SDS-PAGE under non reducing conditions and proved to be more than 95%. ^{99m}Tc Radiolabeling of PR81 and F(ab')_2 fragment were performed using the HYNIC as a chelator and tricine as a co-ligand. The immunoreactivity of the complexes was assessed by radioimmunoassay using MCF7 cells. Biodistribution and imaging studies were performed in female BALB/c mice with breast tumor xenograft after 4, 8 and 24 hs after the preparations injection.

Results

Labeling of PR81 and F(ab')_2 fragment with ^{99m}Tc resulted in a specific activity of $89.2\% \pm 4.7$ and $70.1\% \pm 5.2$ respectively. The immunoreactivity of the ^{99m}Tc -HYNIC-PR81 was $83.2\% \pm 4.7$ and the immunoreactivity of its ^{99m}Tc labeled fragment was $65.2\% \pm 5.1$. The tumors were visualized with high sensitivity after 4 and 24 hrs injections of radiolabeled PR81 and its fragment respectively.

Conclusion

Our comparative study showed that F(ab')_2 fragment of PR81 is much more suitable, rapid and reliable than intact PR81 for diagnosis of breast tumors.



A MULTIPLE WAVELENGTH NIR TRANSMISSION SCANNER FOR SMALL-OBJECT IMAGING

Nikolay UZUNOV^{1,2}, Michele BELLO², Giuliano MOSCHINI², Giuseppe BALDAZZI³, Antonio ROSATO^{4,5}, Maria RONDINA⁵, Pier Carlo MUZZIO^{4,6}

¹*Faculty of Natural Sciences, Shumen University, Shumen, Bulgaria,* ²*National Laboratories of Legnaro, INFN, Legnaro, Italy,* ³*Department of Physics, University of Bologna, Italy,* ⁴*Veneto Institute of Oncology, Italy,* ⁵*Department of Oncology and Surgical Sciences, University of Padua, Italy,* ⁶*Dept of Medical-Diagnostic Sciences and Special Therapies, Univ. of Padua, Italy*

A multiple-wavelength near-infrared (NIR) scanning device has been constructed in the Laboratory for Radiopharmaceuticals and Molecular Imaging (LRMI) at the National Laboratories of Legnaro, INFN, Italy. The scanner uses the transmitted through the objects NIR light at five different wavelengths. The process of scanning is realized by a consecutive positioning of Hamamatsu G9203-256D InGaAs linear image sensor sliding very close to the scanned object. Thus a field of view (FOV) with dimensions 80mm x 50mm can be scanned resulting in a set of five images of the object. The number of object images at different wavelengths provides a multivariate image analysis to be conducted in order to observe small differences in tissue density.

In this article we present first results from the test measurements conducted with the scanner. Spectral analysis of the transmittance of NIR in samples from mice tissues has been conducted. NIR images of mice tissues taken at different wavelengths as well as the resulting images from the multivariate image analysis are discussed.

Comparison between Rotating Slit and Parallel Hole collimation: Influence of Projector Models

Lin Zhou, Kathleen Vunckx and Johan Nuyts
Department of Nuclear Medicine, K.U.Leuven, B-3000, Leuven, Belgium

I. INTRODUCTION

In our previous study [1], the parallel hole (PH) and the rotating slit (RS) collimators were compared based on the contrast-to-noise ratio (CNR) of a uniform phantom. The RS projector that we used in [1] is a "pixellated projector", which considers the detector array as detector pixels, and performs projection and back-projection for each detector pixel individually. This RS projector takes a lot of computation time due to the large number of detector pixels. For practical reasons, a simplified RS projector, which we call "non-pixellated projector", is more preferable. The non-pixellated projector treats all the detectors between the neighbouring collimator septa as one detector element, therefore it works much faster than the pixellated projector. However, the use of the non-pixellated RS projector might lead to a decrease in the CNR due to the loss of information. In this study, we focused on the influence of the RS projector model on the system comparison, investigating to what extent it is reasonable to replace the pixellated projector with the non-pixellated projector for RS.

II. METHODS

In this study, only planar imaging was investigated. An efficient analytical method, i.e., the Fisher information-based method [2]–[4], was used to calculate the CNR of the central point of a 2D flat disk phantom, using PH and RS collimator, respectively. The gain in the CNR (RS over PH) was calculated with the two RS projectors described above. The gains are defined as:

$$\text{Gain}^{\text{pix}} = \text{CNR}_{\text{RS}}^{\text{pix}} / \text{CNR}_{\text{PH}} \quad (1)$$

$$\text{Gain}^{\text{non-pix}} = \text{CNR}_{\text{RS}}^{\text{non-pix}} / \text{CNR}_{\text{PH}} \quad (2)$$

where CNR_{RS} and CNR_{PH} are the CNR yielded with RS and PH collimator, respectively. The superscripts pix and non-pix refer to the pixellated and the non-pixellated RS projector model, respectively.

We used the same system parameters as in [1]. Both PH and RS were equipped with a square detector array of $230.4\text{mm} \times 230.4\text{mm}$. Gain^{pix} and $\text{Gain}^{\text{non-pix}}$ were calculated for different phantom sizes, as well as different phantom-to-detector distances.

III. RESULTS

As shown in Fig. 1, for small phantoms or a large detector distance, two RS projectors yield very similar results, and CNR_{RS} is always higher than CNR_{PH} ($\text{Gain}^{\text{non-pix}} \approx \text{Gain}^{\text{pix}} > 1$). For large phantoms or a small detector distance, we have $\text{Gain}^{\text{non-pix}} < \text{Gain}^{\text{pix}} < 1$, which means that PH outperforms RS anyway, no matter which RS projector is in use.

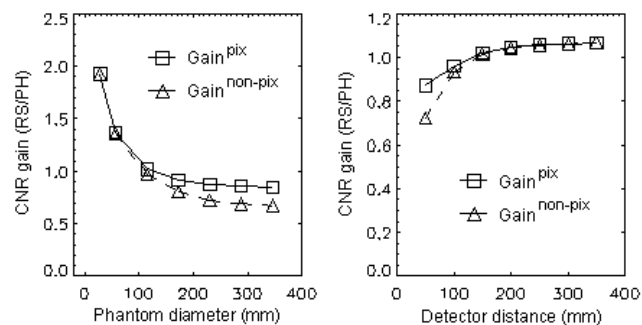


Fig. 1. CNR gains (RS over PH) of the central point of a 2D flat disk phantom. (a) CNR gains as a function of phantom diameter at a small detector distance ($distance = 50\text{mm}$). (b) CNR gains as a function of the detector distance, for a large phantom ($diameter = 230.4\text{mm}$)

IV. DISCUSSION AND CONCLUSION

Suppose the number of detector pixels lying between the neighbouring RS collimator septa is N_d . With a non-pixellated projector, the computation time is N_d times less than with a pixellated projector. However, the information carried in the measurement of a non-pixellated projector is less than that of a pixellated projector. Therefore, every point is reconstructed with lower certainty which results in a higher variance.

With a non-pixellated projector, the noise from the eccentric points is directly propagated to the central point of the phantom during the back-projection. This influence is much stronger when the phantom becomes larger or the phantom is positioned closer to the detector surface.

Based on the comparison result, we suggest that, for large phantom or a small phantom-to-detector distance, PH collimator is recommended. For the opposite cases, RS with a non-pixellated projector is more preferable, since it facilitates the system implementation, saves a lot of computation time and yields very similar results as the pixellated projector.

REFERENCES

- [1] L. Zhou, M. Defrise, K. Vunckx, and J. Nuyts, "Comparison between parallel hole and rotating slit collimation." *IEEE Nuclear Science Symposium Conference Record*, pp. 5530-5539, 2008.
- [2] J. A. Fessler, "Mean and variance of implicitly defined biased estimators (such as penalized maximum likelihood): applications to tomography." *IEEE Trans. Image Processing.*, 5(3), pp. 493-506, 1996.
- [3] J. Qi and R. M. Leahy, "A theoretical study of the contrast recovery and variance of MAP reconstructions from PET data." *IEEE Trans. Med. Imag.*, 18(4), pp. 293-305, 1999.
- [4] K. Vunckx, D. Bequé, M. Defrise and J. Nuyts, "Single and multipinhole collimator design evaluation method for small animal SPECT." *IEEE Trans. Med. Imag.*, 27(1), pp. 36-46, 2008.

